COMP-ECO

PROJECT DELIVERABLE

D1.1 Technical report on research activities and demonstrator

LEAD BENEFICIARY:	AFIT
AUTHOR(S):	Michal Dziendzikowski, Krzysztof Dragan (AFIT)
CONTRIBUTOR(S):	Anna Boczkowska, Kamil Dydek, Paulina Latko-Durałek (WUT), Rafal Kozera, Pawel Duralek (TPF), Otto Bergsma, Nan Tao, Roger Groves (DELFT), Georgios Tzortzinis, Evgenia Madia (DRESDEN)
DATE OF ISSUE:	28.11.2025
DISSEMINATION LEVEL:	PU

https://www.comp-eco.eu/

This project has received funding from the European Union's Horizon Europe research and innovation programme under grant agreement No 101079250

COMP-ECO

DOCUMENT HISTORY

Version and date	Changes
1.0 – 30/10/2025	Draft version (template), developed by Michal Dziendzikowski (AFIT)
1.1 – 15/11/2025	Inputs to respective tasks contributed by WUT, AFIT, TPF, DRESDEN and DELFT
2.0 – 25/11/2025	Pre-final version sent to coordinator for review and approval
2.1 – 28/11/2025	Final version

DISCLAIMER

This project has received funding from the European Union's Horizon Europe research and innovation programme under grant agreement No 101079250

CONTENTS

1. INTRODUCTION

1.1. ABOUT THE COMP-ECO PROJECT

The COMP-ECO project was aiming at improving the research excellence of the Polish Mazovia region-based ecosystem in the field of Fibre-Reinforced Polymer (FRP) multifunctional composites and smart structures. The ecosystem is formed by 3 organizations: Technology Partners Foundation (TPF), Air Force Institute of Technology (AFIT) and Warsaw University of Technology (WUT). These 3 Polish partners were supported by two leading EU universities: Delft University of Technology from the Netherlands and Technische Universität Dresden from Germany.

For 3 years the COMP-ECO partners have jointly implemented exploratory research work to develop a technology for a permanent on-line non-destructive quality assessment of composite structures. For this purpose, 2 possible innovative sensing capabilities were being developed: (1) self-diagnostics capabilities through the introduction of electroconductive carbon nano tubes in the composite's matrix during the manufacturing process and (2) self-sensing capability through embedding PZT sensors, encapsulated in a thermoplastic fibrous material (veils), in the composite structure.

In addition to the research work, the project organized technical workshops aimed on raising the research profile of Mazovian composite community, and management and administrative training workshops to strengthen research management capacities and administrative skills of the Polish partners' administrative staff.

The COMP-ECO activities established and strengthened a regional competence hub formed by TPF, AFIT and WUT, whose increased science and innovation capacities will lead to more ambitious collaboration with top EU research organisations and industry, higher participation in Horizon Europe, and a more attractive educational offer for students and young researchers.

2. RESEARCH PLAN

The research component is included in the Work Package 1, task 1.1 "Exploratory research". The proposed research aims to develop a technology for continuous, non-destructive quality assessment of composite structures using innovative sensing capabilities. These capabilities involve the integration of CNT-doped/neat fibers, veils, or strips, co-developed by WUT-TPF.

Capability 1 focuses on enhancing the self-diagnostic capabilities of the composite by introducing electrically conductive intermediates with added CNTs during production, creating a damage-sensitive sensor. This sensor relies on the conductive percolation network formed by the introduced CNTs, enabling detection of structural deterioration through changes in electrical conductivity as well as heat distribution in the composite material.

Capability 2 involves the deposition of lead zirconate titanate (PZT) sensors encapsulated in veils within the composite structure to monitor the structural condition. These encapsulated sensors provide precise placement and protection during operation, while nondestructive inspection techniques confirm the quality

of the laminate. Based on the defined capabilities of the Project Partners, a research plan was created, consisting of 7 Tasks.

List of research tasks:

- Task 1 - CNT-doped filaments as strain gauges (LEADER: DRESDEN)
- Task 2 - Conductive CNT-doped strips as heater for thermography (LEADER: WUT)
- Task 3 - Conductive CNT-doped veils as delamination sensors. (LEADER: WUT)
- Task 4 - Integration of PZT sensors (LEADER: AFIT)
- Task 5 - Insulation of sensors (LEADER: WUT)
- Task 6 - Connection wires and contact points (LEADER: AFIT)
- Task 7 – Demonstrator (LEADER: DRESDEN)

Mapping of research tasks to the 2 capabilities:

Capability 1: Development of self-diagnostics capabilities of the composite through the introduction of electroconductive CNTs in the composite's matrix during the manufacturing process.	**Capability 2: Embedding PZT sensors, encapsulated in veils, in the composite structure. PZT sensors encapsulation into veils will ensure their accurate placement in the structure and to protect them in service**
Task 1 - CNT-doped filaments as strain gauges, Lead: TU Dresden, participants: TPF, AFIT, WUT	
Task 2 - Conductive CNT-doped strips as heater for thermography, Lead: WUT, participants: TU Dresden, TPF, AFIT	
Task 3 - Conductive CNT-doped veils as delamination sensors, Lead: WUT, participants: AFIT, TPF, TU DRESDEN	
	Task 4 - Integration of PZT sensors. Lead: AFIT, participants: TPF, WUT, TU Delft
Task 5 - Insulation of sensors, Lead: WUT, participants: TPF, AFIT, TU DRESDEN	
Task 6 - Connection wires and contact points. Lead: AFIT, participants: WUT, TU Dresden	
Task 7 - Technology demonstrator, Lead: TU Dresden, participants: TPF, AFIT, WUT, TU DELFT	

The research plan is designed to systematically develop and implement technologies for continuous nondestructive quality assessment of composite structures using innovative measurement capabilities. Each task within the plan addresses specific aspects critical to the successful implementation of the project's goals. Through the effective implementation of these tasks, the project partners will make progress in monitoring the condition of composite structures, contributing to increased maintenance efficiency and safety in various engineering areas.

3. IMPLEMENTATION OF RESEARCH ACTIVITIES

TASK 1 - CNT-DOPED FILAMENTS AS STRAIN GAUGES (LEADER: DRESDEN)

Task 1.1 investigates the feasibility of carbon-nanotube-doped (CNT-doped) thermoplastic filaments as embedded strain-sensing elements for composite structures. The work focuses on verifying fundamental

sensing behavior and assessing whether such filaments can be integrated without degrading laminate performance.

Step 1: Definition of functional requirements.

To support use as in-situ strain sensors, CNT-doped filaments were required to:

- maintain stiffness and strain capacity suitable for integration into GFRP laminates,
- remain less intrusive to the GFRP laminate than conventional strain gauges,
- provide a stable, repeatable piezoresistive response under strain.

Step 2: Filament level characterization.

WUT and TPF manufactured conductive strips with diameters of 0.5mm and 1.0mm using PPS, PET-G, and PA12 matrix materials with a 10% weight fraction. AFIT subsequently tested filaments to determine the suitable matrix and diameter based on electrical performance. Based on preliminary evaluations, PPS filaments demonstrated the most stable conductivity and repeatable piezoresistive behavior, whereas PET-G and PA12 samples showed higher resistance and less reliable strain response.

Three different batches of PPS strips in terms of CNT weight fraction were then provided to TU Dresden for testing. Tests included a length convergence study, as well as examination of the mechanical and piezoresistive response of the filaments.

Based on these results the 4 wt% CNT filaments exhibited the most consistent electromechanical response when tested at a 200 mm free length, showing good linearity in the ΔR/R–ε trend and low deviations. At this configuration, gauge factors were around k ≈ 2, representing the most reliable sensing performance within the tested range. This setup was therefore selected as the baseline configuration for subsequent laminate integration. The ΔR/R–ε behavior for this configuration is shown in the plot below:

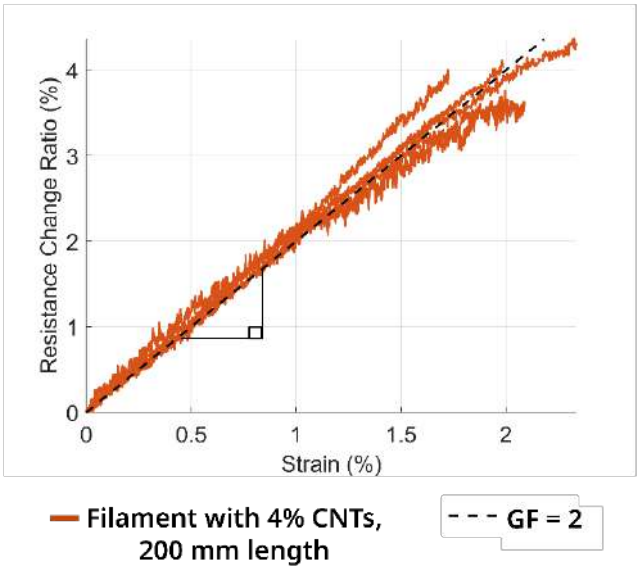

Figure 1: Indicative resistance change ratio vs strain.

Step 3: Specimen manufacturing & Quality assessment.

GFRP specimens were produced using a controlled autoclave process, incorporating CNT-doped filaments either:

- embedded within the laminate at 7/8 of the stack,
- positioned on the surface at 8/8 of the stack, or
- embedded at 7/8 of the stack after plasma treatment to explore adhesion.

Reference specimens with commercial strain gauges were manufactured in parallel.

Quality verification included microscopy and thermal analysis to confirm uniform cure and proper filament placement. No manufacturing-induced defects affecting the filaments were observed. The indicative figures of the quality assessment can be seen below in Figure 2.

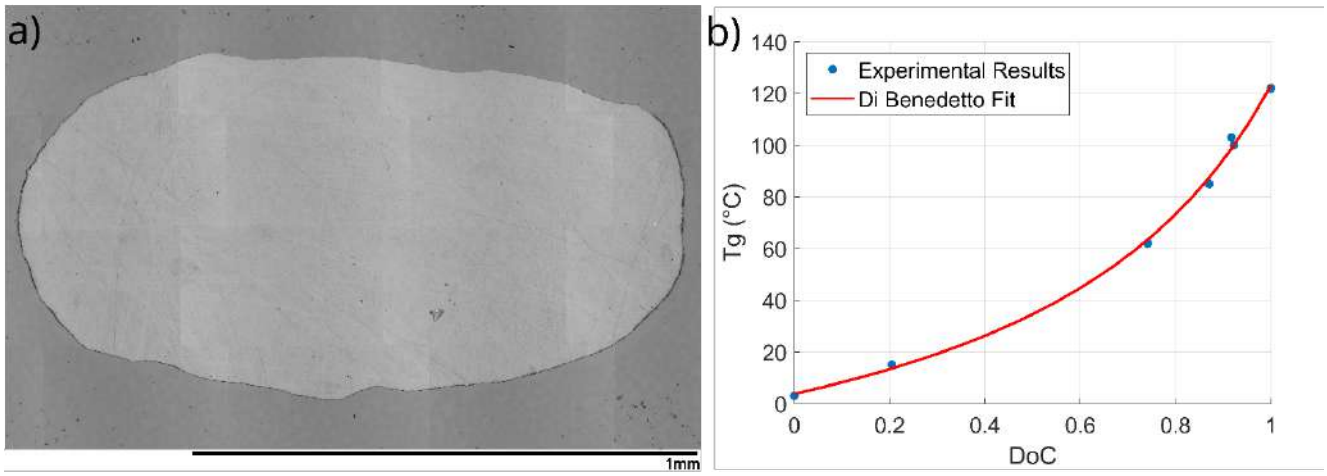

Figure 2: Avalysis of the created specimens: (a) Microscopy and (b) Fitted plot of Tg evolution as a function of the degree of cure.

Step 4: Specimen testing.

Mechanical performance was assessed through standardized three-point bending tests. Key outcomes:

- Embedded CNT filaments did not adversely affect laminate stiffness.
- Plasma-treated specimens exhibited a slight increase in flexural modulus, whereas strain-gauge specimens a slight decrease.

Piezoresistive monitoring during bending showed:

- embedded filaments had a stable but moderate sensitivity (GF ≈ 0.3),
- surface-mounted filaments exhibited a slightly higher sensitivity (GF ≈ 0.4),
- plasma-treated filaments depicted a non-linear response, suggesting altered strain-transfer mechanisms.

Indicative mechanical and piezoresistive results of series with embedded and plasma treated filaments can be seen below on Figure 3.

Overall, the results demonstrate that CNT-doped PPS filaments can function as integrated strain sensors, though additional optimization is needed to improve sensitivity and achieve gauge factors closer to commercial standards.

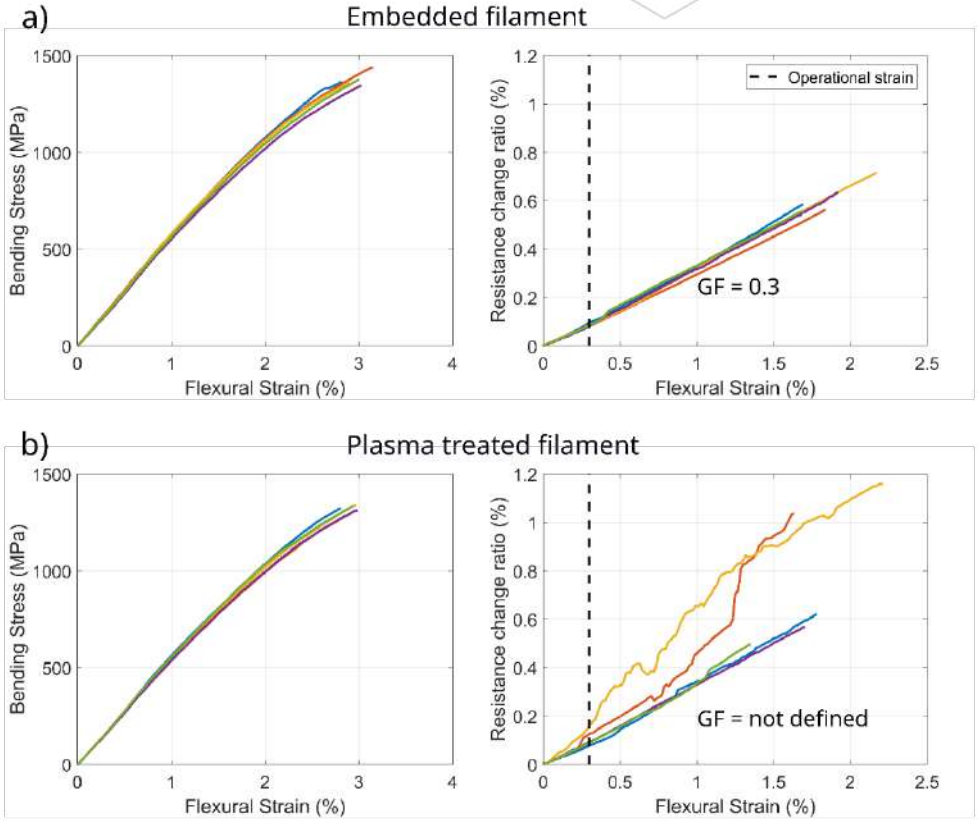

Figure 3: Mechanical and piezoresistive results from testing of A) series with embedded filaments, b) series with plasma treated filaments.

TASK 2 - CONDUCTIVE CNT-DOPED STRIPS AS HEATER FOR THERMOGRAPHY (LEADER: WUT)

Introduction:

Glass Fiber Reinforced Polymer (GFRP) composites have become indispensable in various industrial applications due to their numerous advantages over traditional materials, such as high strength-to-weight ratio, outstanding thermal and electrical insulation, and superior corrosion resistance. These properties make GFRPs highly valuable in aerospace, automotive, and civil infrastructure sectors, serving as lightweight, durable alternatives to conventional materials. However, despite their robustness, GFRP structures are susceptible to fatigue loads, impact loads, and environmental erosion over long-term service. This vulnerability necessitates significant efforts towards ensuring these materials' in-service reliability and safety. Recent advancements aim to embed innovative sensing technologies within the GFRP matrix, enabling real-time damage detection and structural health monitoring.

Due to the complex composite microstructure, the manufacturing process of GFRP can generate defects such as voids, fibre misalignment, waviness, dry spots, and resin-rich areas. These defects or in-service damage can cause delamination, debonding, matrix cracks or fibre breakage during composite parts exploitation, which finally leads to component failure. Hence, it is crucial to evaluate the condition of composite internal parts to avoid catastrophic failure.

Infrared Thermography (IRT) is one of the most favorable NDT techniques, that detects the infrared energy emitted by tested objects and visualises it to provide information about the sample temperature. It can be divided into passive and active thermography, and both modes have been used to investigate composite materials. In passive thermography, thermal radiation naturally emitted by objects is detected. In contrast, in active thermography, an external heating source is used to stimulate heating flow in material to detect defects and damages. The heating flow in materials can be activated by various sources: optical excitation, Eddy currents, electrical current, magnetic induction, microwaves, ultrasound or mechanical methods.

The goal of this task is to replace the most commonly used halogen lamp as the heat source in active thermography through efficient heaters (in the form of strips) based on CNTs doped thermoplastic material.

Materials:

Heaters: Fortron® PPS was used as a polymer matrix to produce PPS/MWCNT nanocomposites, whereas MWCNTs with the trade name NC7000 from Nanocyl. The average diameter of an MWCNT is 9.5 nm, its length is 1.5 µm, and its purity >95%. Additionally, Nanocyl manufactured and delivered masterbatch in the form of pellets, contained 10 wt% MWCNT.

Prepreg: Prepreg GlasHEXPLY M9.6GF is a hotmelt, thermosetting, moderate tack epoxy resin matrix, specifically designed for prepreg applications at which short cure cycles of 100°C and above are required. M9.6GF can be used for the manufacture of large industrial components and is suitable for the cure of thin and thick sections. M9.6GF exhibits a long out-life at ambient conditions.

Manufacturing:

- Autoclave method–vacuum bag – during internships in TU Dresden
- Laminate layup: [45/0/-45/90]s – 8 layers in total - ASTM D7136
- Heaters insertion place: in the middle, on the surface, between 2nd and 3rd layer
- Number of heaters: 6 and 8
- Total number of laminates: 9

Results:

Connection CNT-doped strips with cables (WUT+AFIT+TU Dresden)

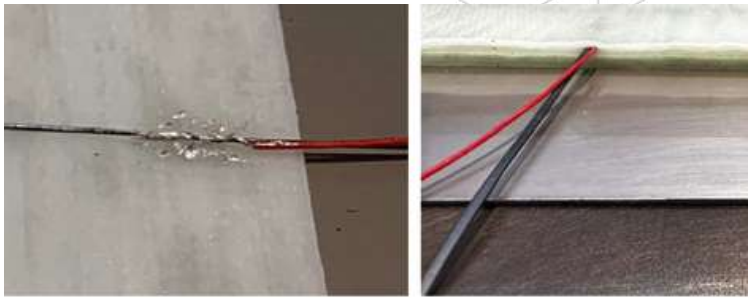

Figure 4 Connection CNT-doped strips with cables

The electrical contact within the system is ensured by the use of a conductive epoxy adhesive containing silver particles. This adhesive maintains a stable resistivity level, with no significant increase observed after curing, ensuring reliable conductivity throughout the structure. Additionally, high-temperature cable insulation is employed to prevent any melting or degradation during the autoclave process, ensuring the integrity and performance of the system under elevated temperatures. These measures collectively contribute to the robustness and reliability of the electrical connections within the composite structure, essential for its functionality and long-term durability.

SEM observations (WUT):

The effect of introducing CNT-doped strips on the microstructure of GFRP laminates was studied using a scanning electron microscope (SEM, TM3000, Hitachi, Japan). Adhesion at the sensor-epoxy resin interface was also analyzed. The samples of 10 × 10 mm dimensions were sanded and polished using two diamond slurries. Afterward, samples were coated with an Au–Pd electroconductive layer using 1.5 kV voltage, 12 mA current, and 90 s.

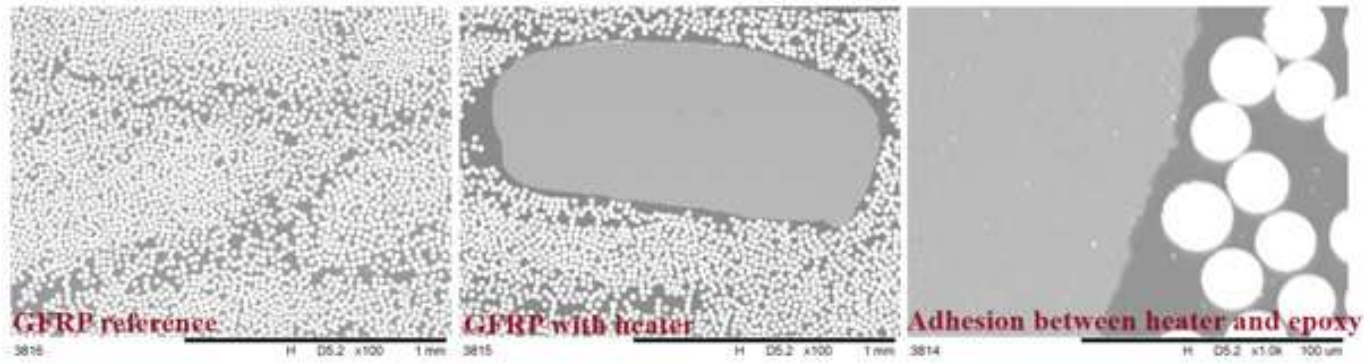

Figure 5 SEM observations

SEM observations confirmed that the autoclave laminate fabrication process went well - no defects were noted in the structure of both the reference and laminates with heaters. In addition, good adhesion at the heater-epoxy resin interface was confirmed.

DMA analysis (WUT):

Dynamic mechanical analysis (DMA) was carried out to evaluate the viscoelastic properties of GFRPs, as well as the impact of introducing CNT-doped sensors into their structure. From the resulting curves, the glass transition temperature (Tg) was determined. The analysis used a DMA Q800 analyzer (TA Instruments, New Castle, DE, USA) in dual cantilever mode, following the ASTM D7028 standard. The temperature range was set from 0 to 160 °C, with

a heating rate of 3°C/min, a frequency of 1 Hz, and an amplitude of 20 µm. The test specimens measured 60 mm in length and 10 mm in width.

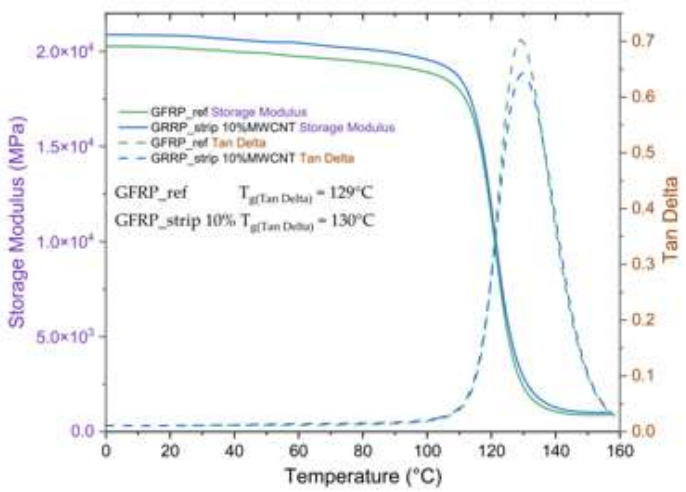

Figure 6 Analysis results

Despite the introduction of CNT-doped strips, there was no observed effect on the glass transition temperature (Tg) of the composite material. However, an increase in the stiffness of the glass fiber-reinforced polymer (GFRP) was noted after the insertion of CNT-doped strips, indicating a positive impact on mechanical properties. Additionally, it was confirmed that the crosslinking process was executed correctly, ensuring the structural integrity and performance of the composite material.

Current-voltage parameters during induction (WUT+AFIT):

Number of heaters	Sensor placement	Connection type	After impact	Temperature (°C)	Voltage (V)	Current (A)	Power (W)
6	Between 4th and 5th layer (mid)	Copper cable	No	35	29.77	0.342	10
	Between 4th and 5th layer (mid)		Yes	35	29.99	0.338	10
6	Between 2nd and 3rd layer (2/3)	Copper cable	No	35	30.01	0.257	8
	Between 2nd and 3rd layer (2/3)		Yes	35	30.01	0.195	5
8	Between 2nd and 3rd layer (2/3)	Copper cable	No	35	27.01	0.38	10
	Between 2nd and 3rd layer (2/3)		Yes	35	30.01	0.293	8
8	Between 4th and 5th layer	Copper cable	No	35	29.55	0.347	10
	Between 4th and 5th layer		Yes	35	29.77	0.337	10

Impact test (WUT):

To verify the possibility of using CNT-doped strips as heaters in NDT techniques, an impact test was performed in accordance with the ASTM D7136 standard, introducing a defect in the structure of the fabricated GFRPs. The

impact energy was 30J, and the impactor weighed 5,526kg. However, it was observed that when the strips were placed on the surface, they sustained damage after the impact event.

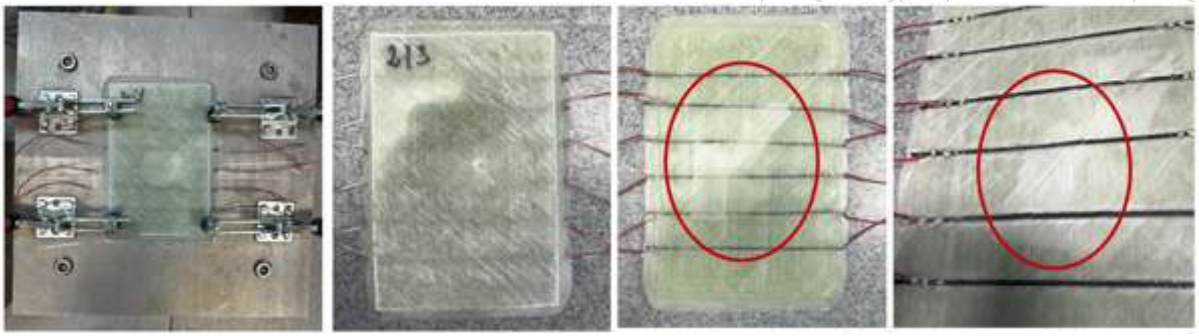

Figure 7 Specimens after impact test

Thermography (AFIT+WUT):

Active thermography studies were performed using an infrared camera (FLIR SC7500, resolution 320 × 256 pixels, 10 frames per second, and a spectral band of 1.5 to 5.1 μm) to record the temperature field on the sample's surface. A high-voltage power supply AU—15P40 was used to generate thermal energy from CNT-doped heaters inside the GFRP laminates. In addition, the resistance of each of the introduced sensors was tested before and after the impact test using a standard multimeter.

Sample: 6 heaters, place: in the middle, before impact 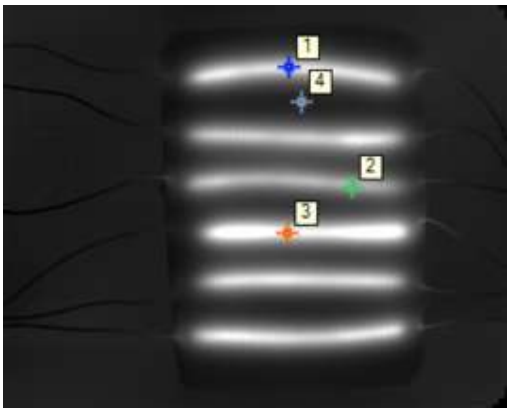	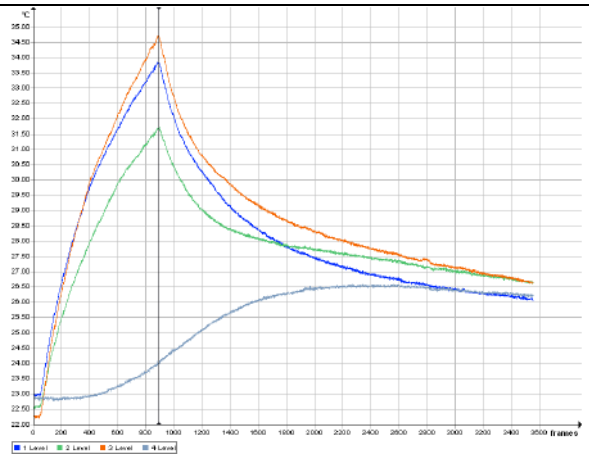

Sample: 6 heaters, place: in the middle, after impact

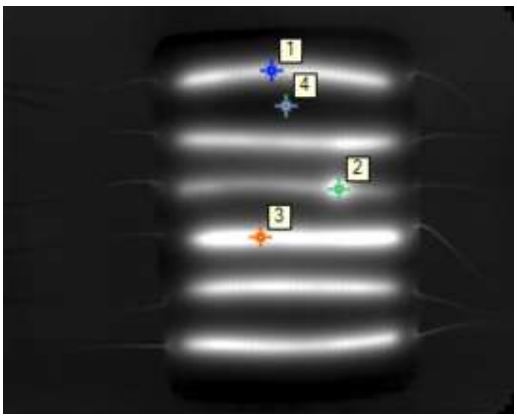

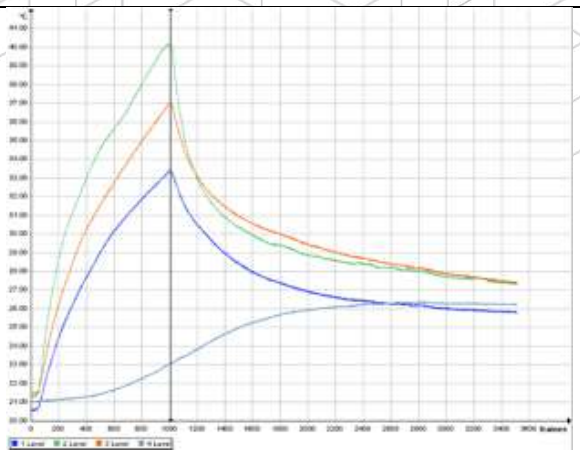

Sample: 6 heaters, place: between 2nd and 3rd layer, before impact

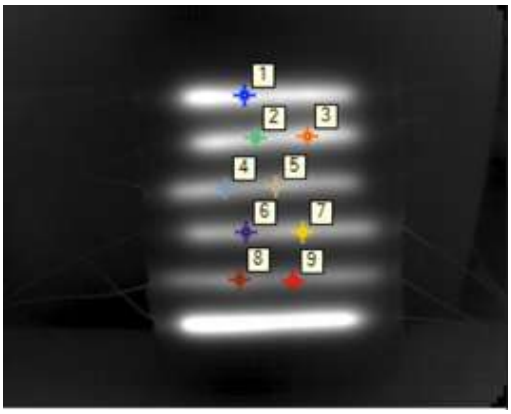

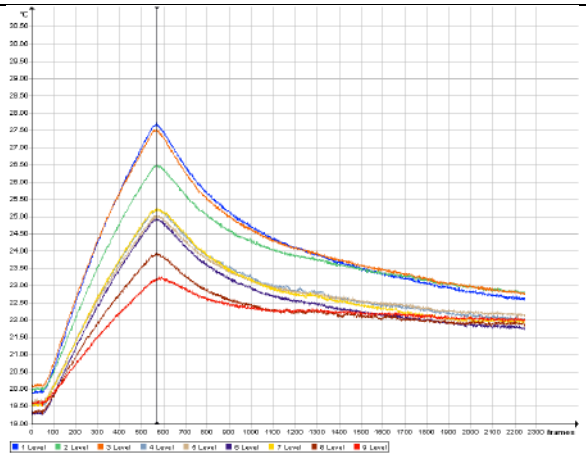

Sample: 6 heaters, place: between 2nd and 3rd layer, after impact

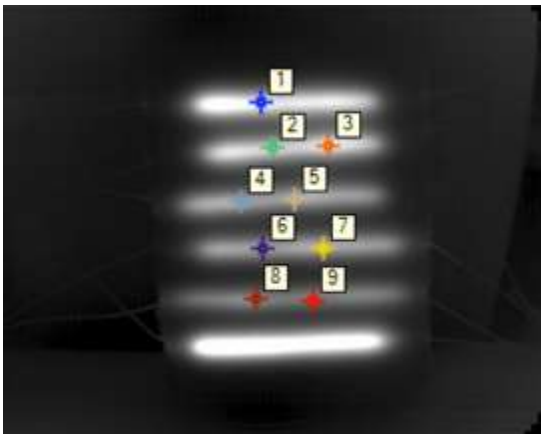

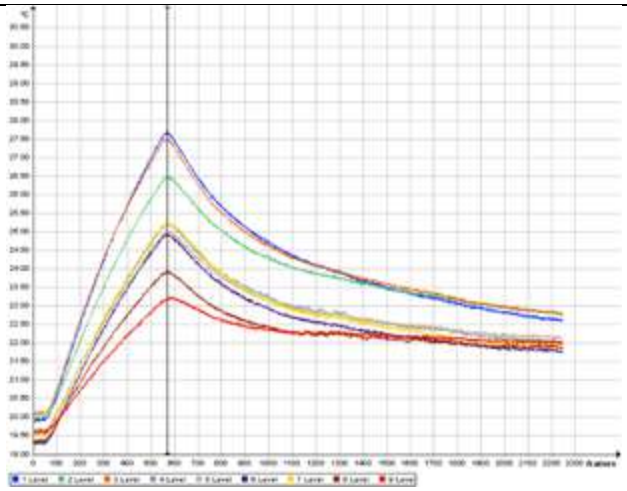

Sample: 8 heaters, place: in the middle, before impact

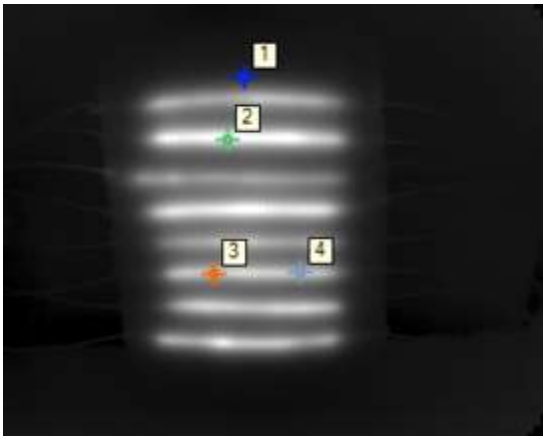

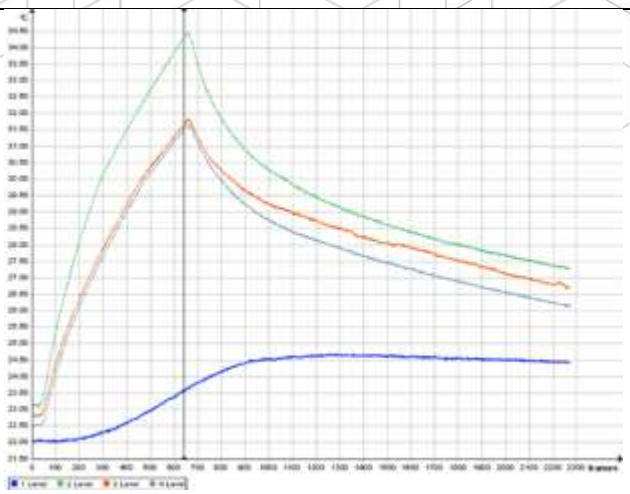

Sample: 8 heaters, place: in the middle, after impact

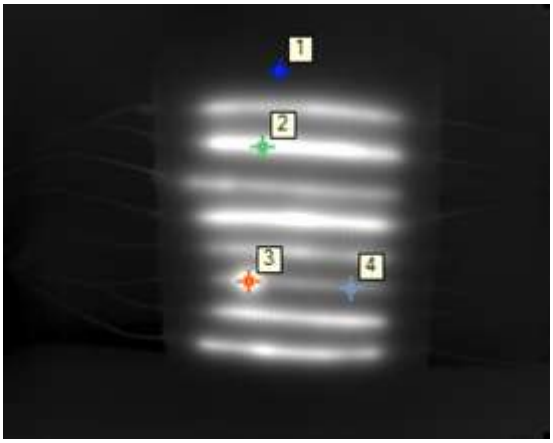

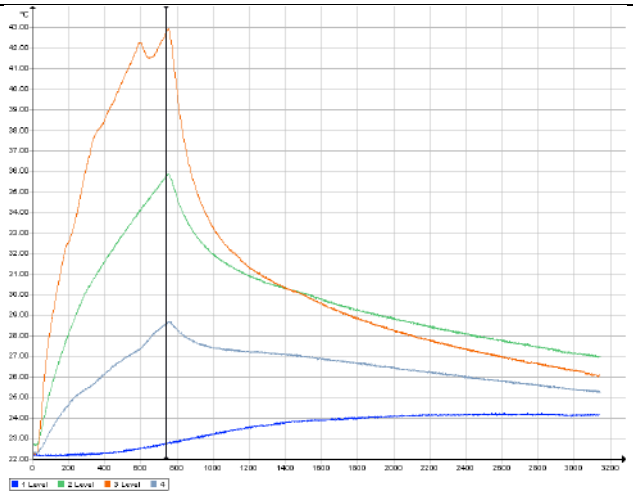

Sample: 8 heaters, place: between 2nd and 3rd layer, before impact

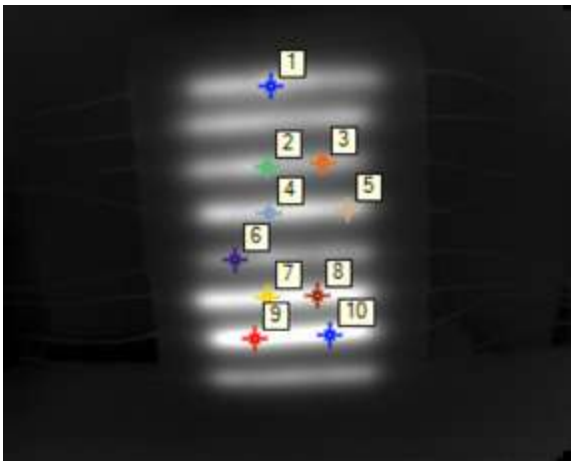

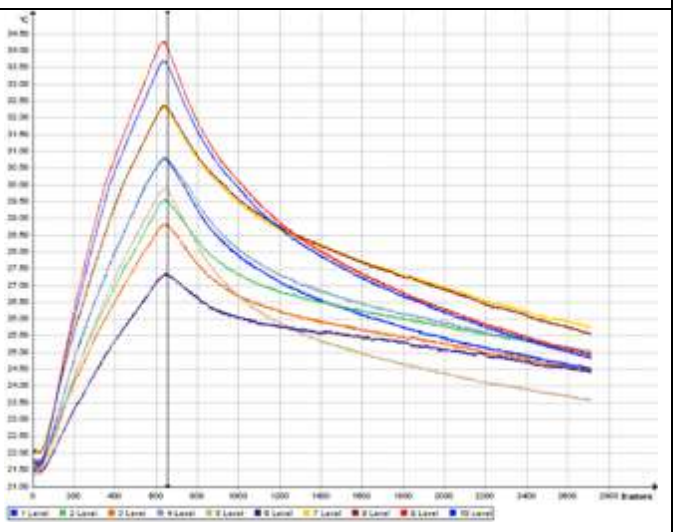

Sample: 8 heaters, place: between 2nd and 3rd layer, after impact	
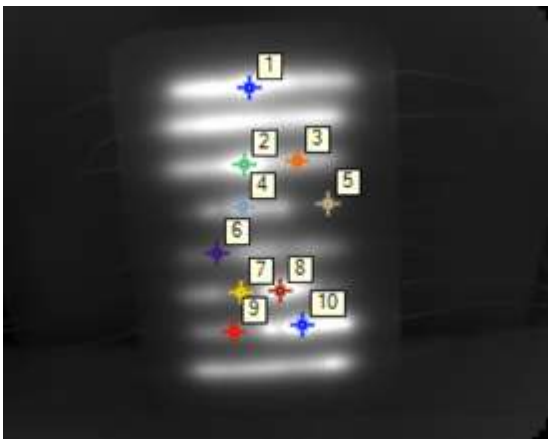	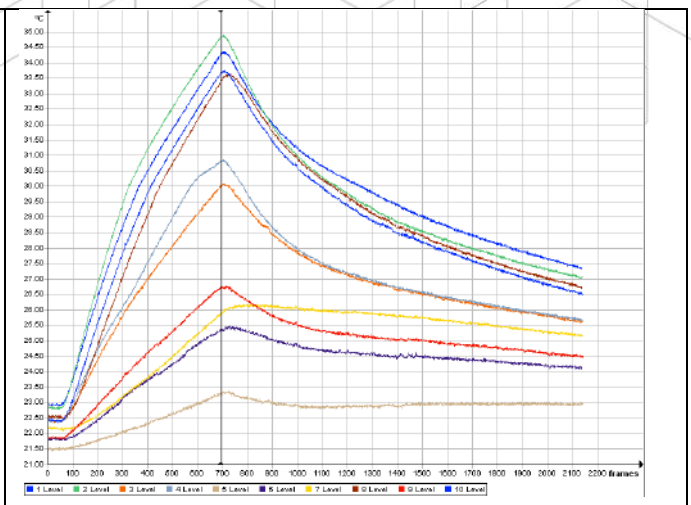

The CNT-doped strips developed as part of TASK2 can be effectively used in active thermography as an internal heat source. In addition, they allow the identification of damage (delamination) through visible brighter spots that occur along the length of the strip and are associated with differences in heat dissipation in the material.

NDT test (AFIT):

Ultrasonic testing was conducted on the laminates both before and after the impact test using the Dolphicam 2 device. This advanced non-destructive testing (NDT) tool provides high-resolution imaging and accurate analysis. For this work, an amplitude mode (AMP) was used, and the test parameters were as follows: Transducer Frequency 2,5 MHz, Analog Gain 0.0 dB, Aperture 16, Signal Averaging 2, Pulse Length 140 ns, Transducer Pitch 0.25 mm.

Sample: 6 heaters, place: in the middle, before impact	
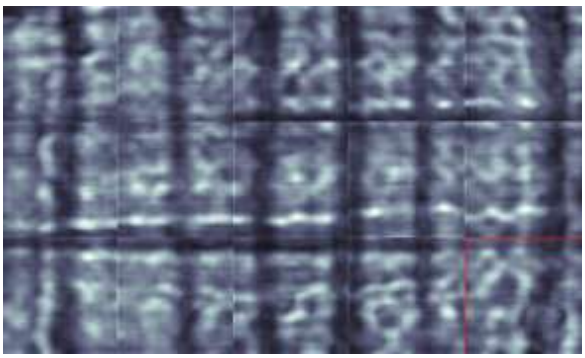	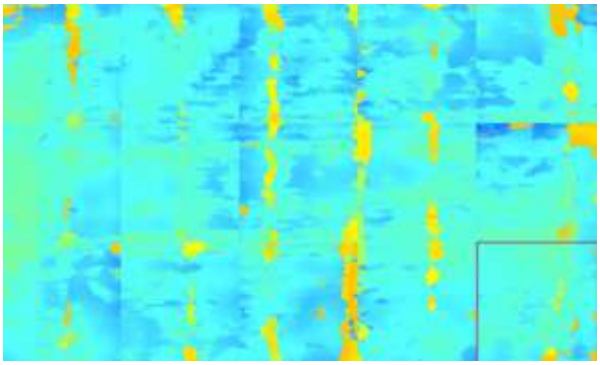

Sample: 6 heaters, place: in the middle, after impact	
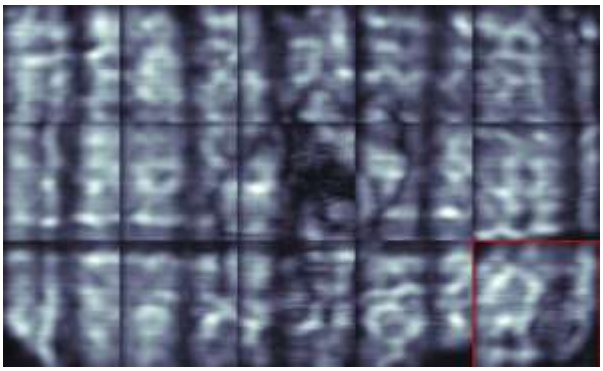	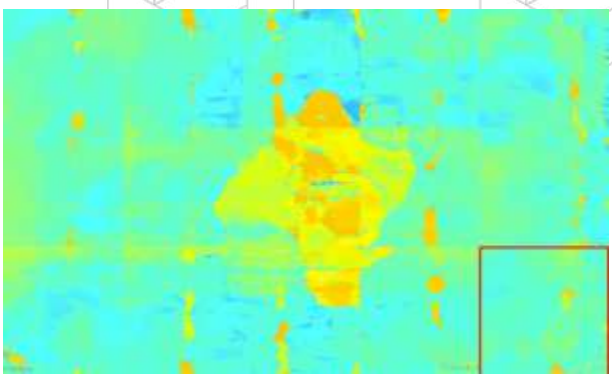
Sample: 6 heaters, place: between 2nd and 3rd layer, before impact	
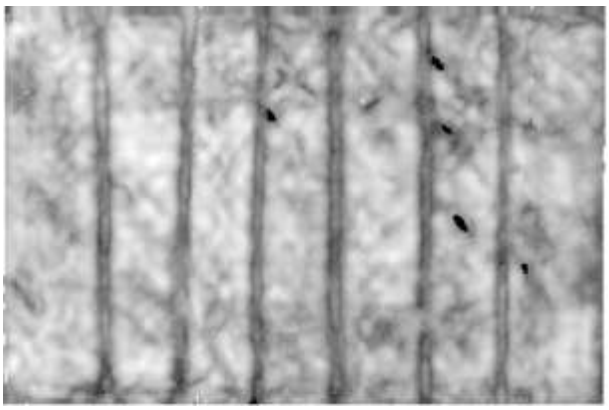	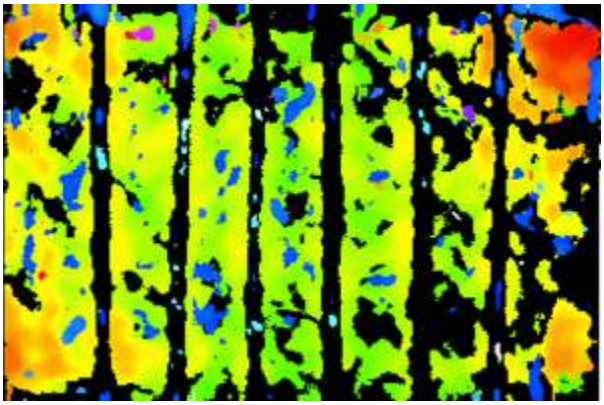
Sample: 6 heaters, place: between 2nd and 3rd layer, after impact	
	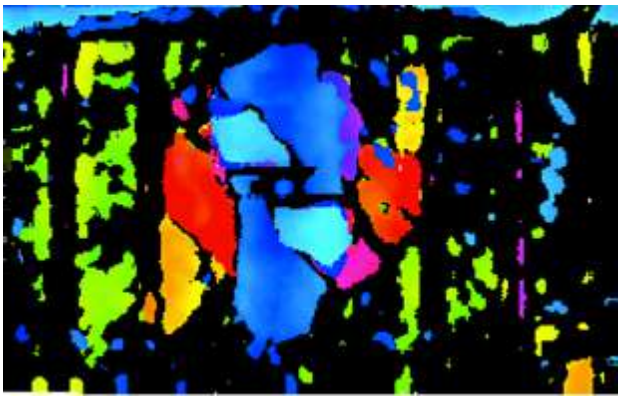

Sample: 8 heaters, place: in the middle, before impact 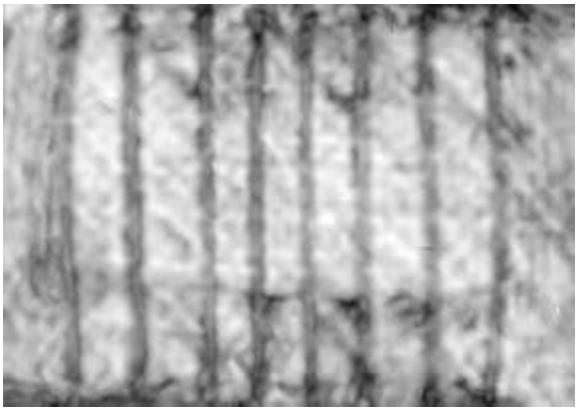	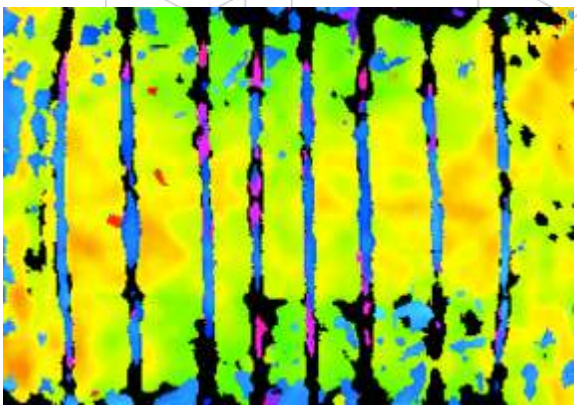
Sample: 8 heaters, place: in the middle, after impact 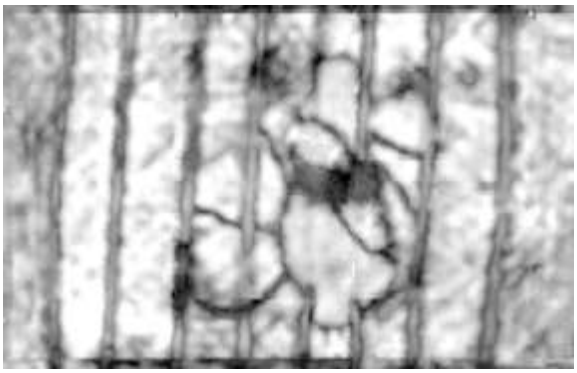	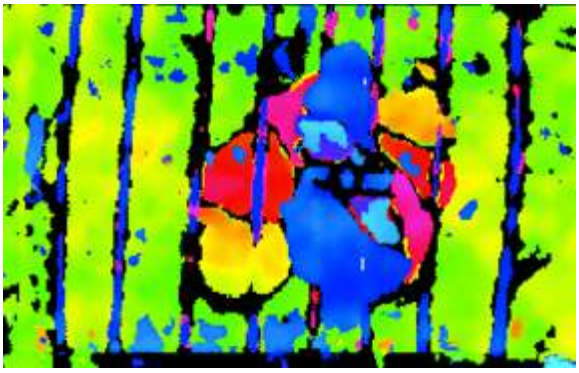
Sample: 8 heaters, place: between 2nd and 3rd layer, before impact 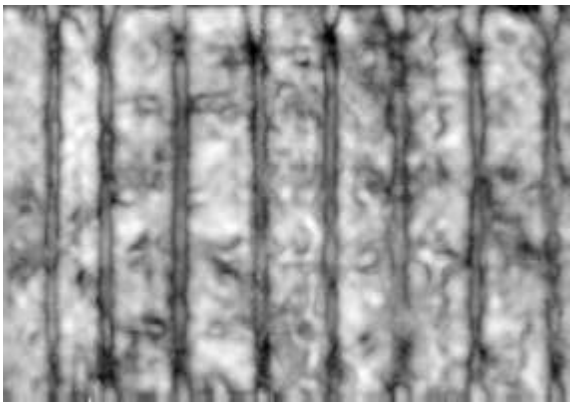	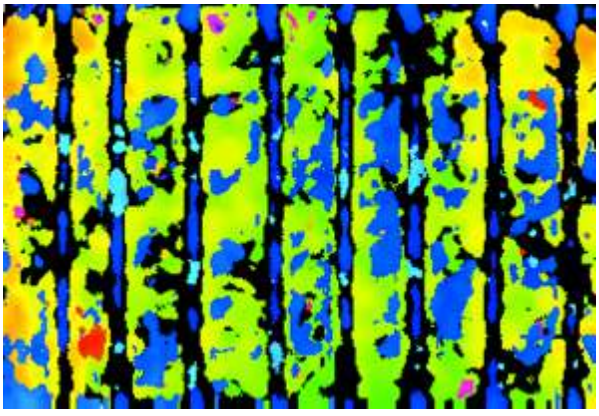

Sample: 8 heaters, place: between 2nd and 3rd layer, after impact	
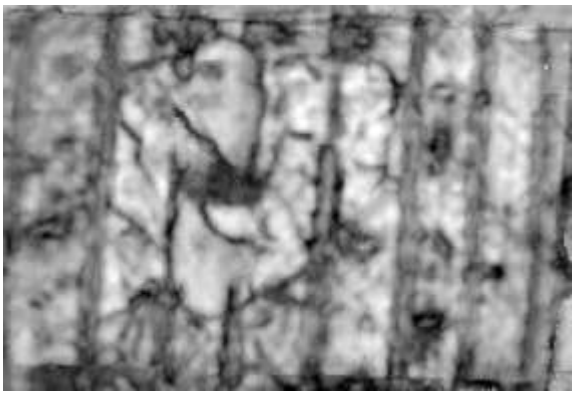	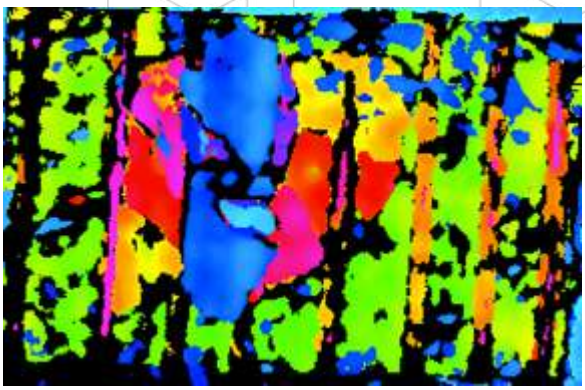

Ultrasound technology allows for the identification of the location of the CNT strip, as well as the area of delamination in samples after impact.

Sheargraphy (DELFT):

In this study, one channel of previously developed 3D shearography system with a focus on the out-of-plane deformation was adapted for the inspection. This was achieved by adjusting one shearography camera perpendicular to the test specimens. Shearography tests were performed before and after the impact test of the specimens. During a shearography experiment, the specimen was heated by embedded CNT strips for 240 s. The speckle interferograms were captured continuously before heating, during heating and during cooling of the specimen. Phase maps were obtained by comparing phase differences of the speckle interferograms at two deformation states (in the heating or cooling), and phase compensation process was performed to remove overall or global deformation for improving defect detection.

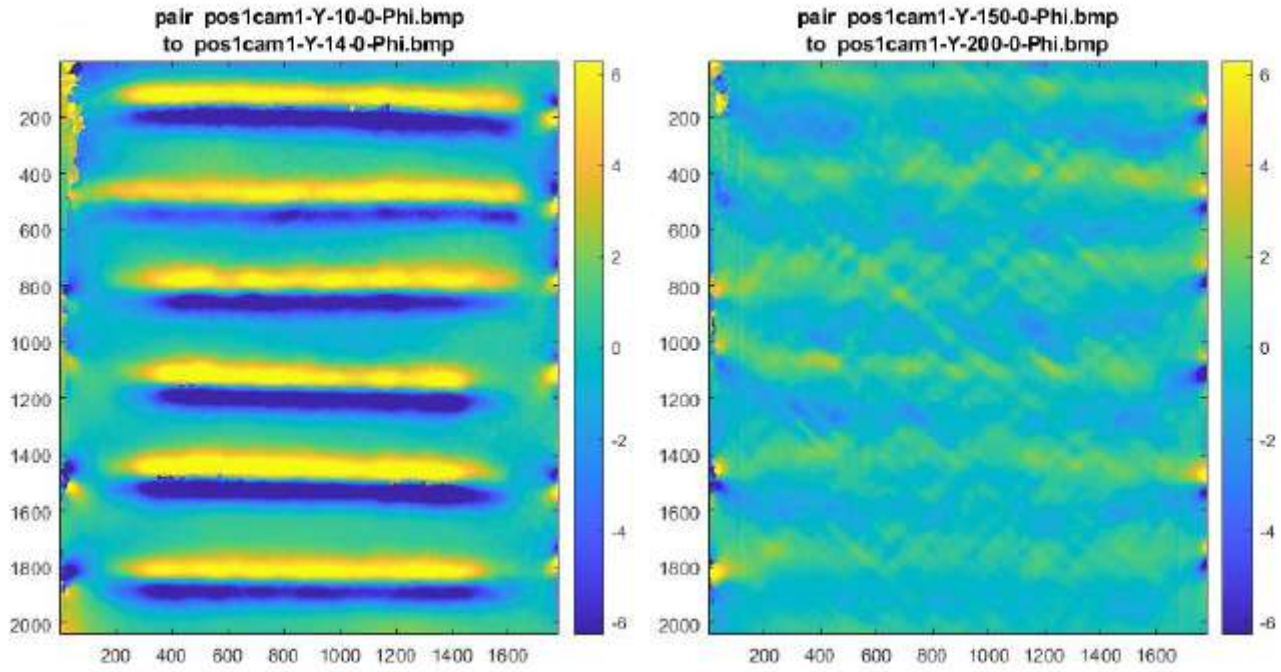

Figure 8 Sample: 6 heaters, place: between 2ndand 3rdlayer, before impact

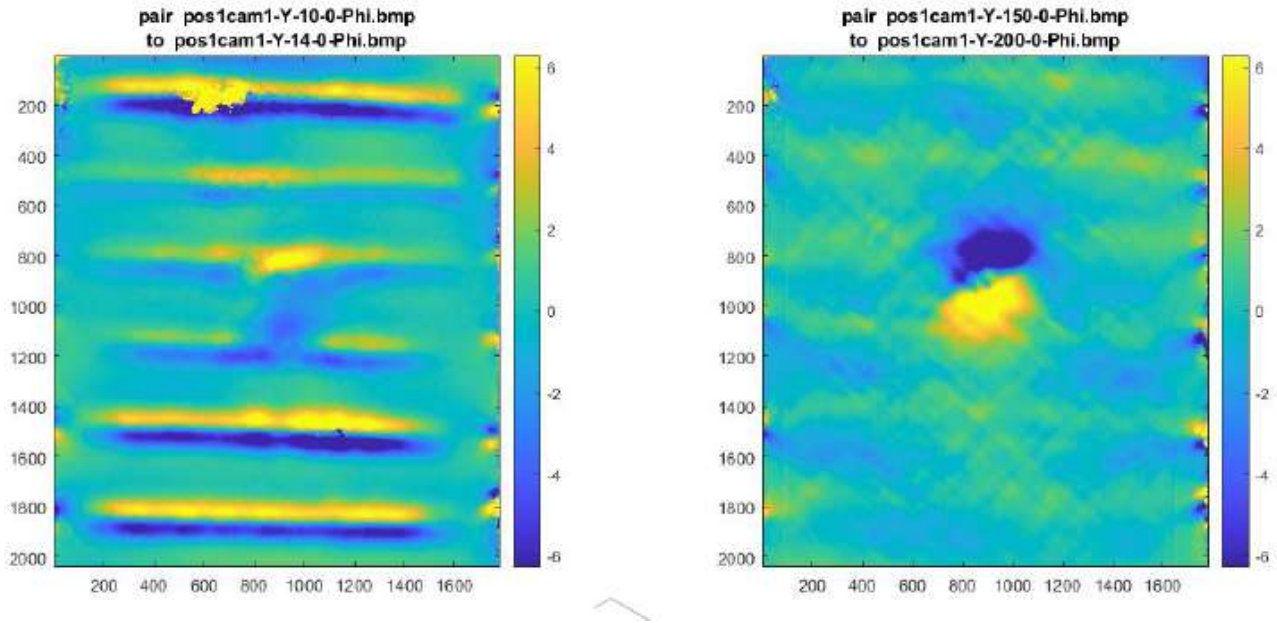

Figure 9 Sample: 6 heaters, place: between 2ndand 3rdlayer, before impact

Summary

This research investigated the integration and performance of CNT-doped thermoplastic strips embedded within glass fibre reinforced polymer (GFRP) laminates to function as internal heaters

for active thermography in non-destructive testing (NDT). The overarching goal was to replace traditional external heating sources—such as halogen lamps—with lightweight, energy-efficient, internally embedded heating elements, enabling improved defect detection and real-time structural health monitoring.

A series of characterization techniques confirmed the structural and functional integrity of the developed heating system. The electrical connections, formed using silver-filled conductive epoxy, demonstrated stable resistivity before and after curing, while high-temperature cable insulation effectively protected the interfaces during the autoclave cycle. SEM observations revealed that both reference and heater-integrated laminates were free of voids and microstructural defects, and exhibited excellent adhesion between the CNT-doped strips and the epoxy resin matrix. Dynamic mechanical analysis further confirmed that the incorporation of heaters did not affect the glass transition temperature of the composite; instead, a beneficial increase in stiffness was observed, indicating that the integration of CNT-doped strips does not compromise, and may even enhance, mechanical performance.

Impact tests performed according to ASTM D7136 introduced controlled damage to evaluate the ability of the heaters to support damage detection. Strips placed on the laminate surface were damaged during impact, while strips embedded between plies remained intact and fully functional. Active thermography demonstrated that the embedded CNT heaters provide consistent and uniform heat generation. The induced thermal fields enabled clear visualization of delamination areas, observable as brighter regions along the heater axis corresponding to altered heat dissipation paths. These results confirmed that the heaters provide a reliable and sensitive internal excitation source for defect detection. Complementary ultrasonic testing with the Dolphicam 2 system validated the location of heaters and revealed the extent of impact-induced damage. Differences between pre- and post-impact scans allowed accurate mapping of delamination zones. Shearography experiments, conducted using an adapted out-of-plane 3D shearography setup, further confirmed the capability of CNT-based heaters to induce thermal deformation fields sufficient for identifying subsurface defects. Phase maps obtained during heating and cooling cycles clearly visualized damage regions and allowed separation of global deformation from localized defect-related signals.

Collectively, the results of this work demonstrate that CNT-doped thermoplastic strips developed in Task 2 are highly effective as embedded heating elements for multifunctional composite structures. They enable reliable, repeatable, and spatially controlled thermal excitation for multiple NDT techniques, including active thermography, ultrasonics, and shearography. The integration of these heaters does not degrade laminate quality or thermo-mechanical properties, and when placed inside the composite layup, they remain operational even after impact events. This technology opens the way for smart composite components with built-in diagnostic capabilities, offering improved inspection performance, reduced energy consumption, and enhanced suitability for real-time structural health monitoring in aerospace, automotive, and infrastructure applications.

TASK 3 - CONDUCTIVE CNT-DOPED VEILS AS DELAMINATION SENSORS. (LEADER: WUT)

The main goal of Research Task 3 was to validate the usage of CNT-doped veils as the delamination sensors for fiber-reinforced composites. CNT-doped veils belong to the group of nonwoven fabrics where fibers are randomly oriented and bonded thermally during the production process call melt-blown. The idea is to embed the CNT-doped veils directly as the interlayers in glass-fiber reinforced polymers (GFRP), showing decreased electrical resistance after damage. However after preliminary examinations it was found that electrical resistivity of the CNT-doped veil is too low ($R=10^{10}\ \Omega$) to be applied as sensors. Therefore, it was decided to increase the electrical conductivity of the veils by the metallization process. For the comparison also pure veils (without carbon nanotubes) were metallized. Table 1 contain the list of the metallized veils.

Electroless deposition/metallization allows deposition on non-conductive and low-conductive substrates. It involves sensitizing the surface with a $SnCl_2$ solution and activating it with a $PdCl_2$ catalyst. The catalyst allows the reaction to start on the substrate surface. The reaction then proceeds autocatalytically until the components are completed. In this case, a Ni-P coating is deposited with a phosphorus content of up to 5%. The electroless deposition includes a few steps:

1. Cleaning and degreasing 5 min
2. Rinsing with distilled water, 5min
3. Sensibilization $SnCl_2$/HCl, 10 min
4. Rinsing with distilled water, 10min
5. Activation $PdCl_2$/HCl, 5 min
6. Rinsing with destilled water, 10 min
7. Immersion in electroless bath, $NiSO_4$, NaH_2PO_2/Gly/ thiourea/pH=8.5, 8 minutes
8. Rising with destilled water, 10 min

For that first trials, the metallization process was conducted with lower concentration of acetone uses for cleaning the veil' surface before further steps. The metallization process of veils no1 and no2 underwent well and, and a nicel-phospohurs layer was created on the macroscale. It was visible, especially for the neat coPA veil, which was white before metallization and grey after (Figure 1 a and b) . However, the main problem was that veils easily moved during step immersion in electroless bath, causing deformation, especially for the coPA veil. The microscopic observations of the veil's structure were made using the Scanning Electron Microscope (SEM, Hitachi 3000) to check how the metallization process went. As presented in the images in Figure 2 and Figure 3, the analyzed veils possess different structures related to the melt-blown manufacturing conditions used to produce veils. In the case of coPA veils, the structure is dense, and the fibres are thinner than for the PPS veil, in which fibers are thicker, and the structure is more porous. After metallization, the coPA veil became grey, suggesting the formation of the Ni-P layer, visible in the microscale as the white covering of the fibres (Figure 2). The metallization process of the PPS veil was not as homogenous because only some fibres were covered by the Ni-P layers (Figure 3). Moreover, the formed layer was brittle in both cases but to a higher extent for the PPS veil. Probably, CNT hampers the metallization process due to the difference in the surface tension of both veils.

In the second trials, the metallization process was conducted in more concentrated acetone and with longer cleaning time. Unfortunately, veils made of coPA became brittle immediately after immersing in concentrated acetone. Contrary to veils made of PPS which remain unchanged. Therefore, further metallization steps were performed only for veils of PPS containing 1wt% of CNT (also with graphite)

having various areal weight. The veils of PPS+1wt% CNT (no 7 and no8 from Table 1) before and after metallization was showed in Figure 3. Despite the differences in the areal weight, in both types of veils the visible metallized layer was formed. The SEM images that most of the fibres were covered by Ni-P coating however in some places the layer is brittle. These two veils will be used to manufacture composite panels for further tests.

Table 1. *The list of metallized veils.*

No	Polymer	CNT content [wt%]	GSM [g/m^2]	Metallization process
1	coPA 1657	neat	16	OK
2	PPS	1	25	OK
3	coPA 1657	3	20	Veil became brittle after cleaning with acetone due to too high concentration
4	coPA 1657	1	17	
5	PPS	1	25	OK even at higher concentration of acetone
6	PPS	1 + 3.6% graphite	42	
7	PPS	1	25	
8	PPS	1	60	

Figure 1 shows the veils before and after the metallization process. The whole process for both veils went well, and a nicel-phospohurs layer was created on the macroscale. It was visible, especially for the neat coPA veil, which was white before metallization and grey after (Figure 1 a and b) . A good point is that veils were not dissolved in the used solvents. However, the main problem was that veils easily moved during step no7, causing deformation, especially for the coPA veil.

Figure 10. From the left: neat coPA veil before metalization; coPA veil after metalization; PPS veil with 1wt% CNT before metallization; PPS veil with 1wt% CNT after metallization.

The microscopic observations of the veil's structure were made using the Scanning Electron Microscope (SEM, Hitachi 3000) to check how the metallization process went. As presented in the images in Figure 2 and Figure 3, the analyzed veils possess different structures related to the melt-blown manufacturing conditions used to produce veils. In the case of coPA veils, the structure is dense, and the fibres are thinner than for the PPS veil, in which fibers are thicker, and the structure is more porous. After metallization, the coPA veil became grey, suggesting the formation of the Ni-P layer, visible in the microscale as the white covering of the fibers (Figure 2). The metallization process of the PPS veil was not as homogenous because only some fibers were covered by the Ni-P layers (Figure 3). Moreover, the formed layer was

brittle in both cases but to a higher extent for the PPS veil. Probably, CNT hampers the metallization process due to the difference in the surface tension of both veils.

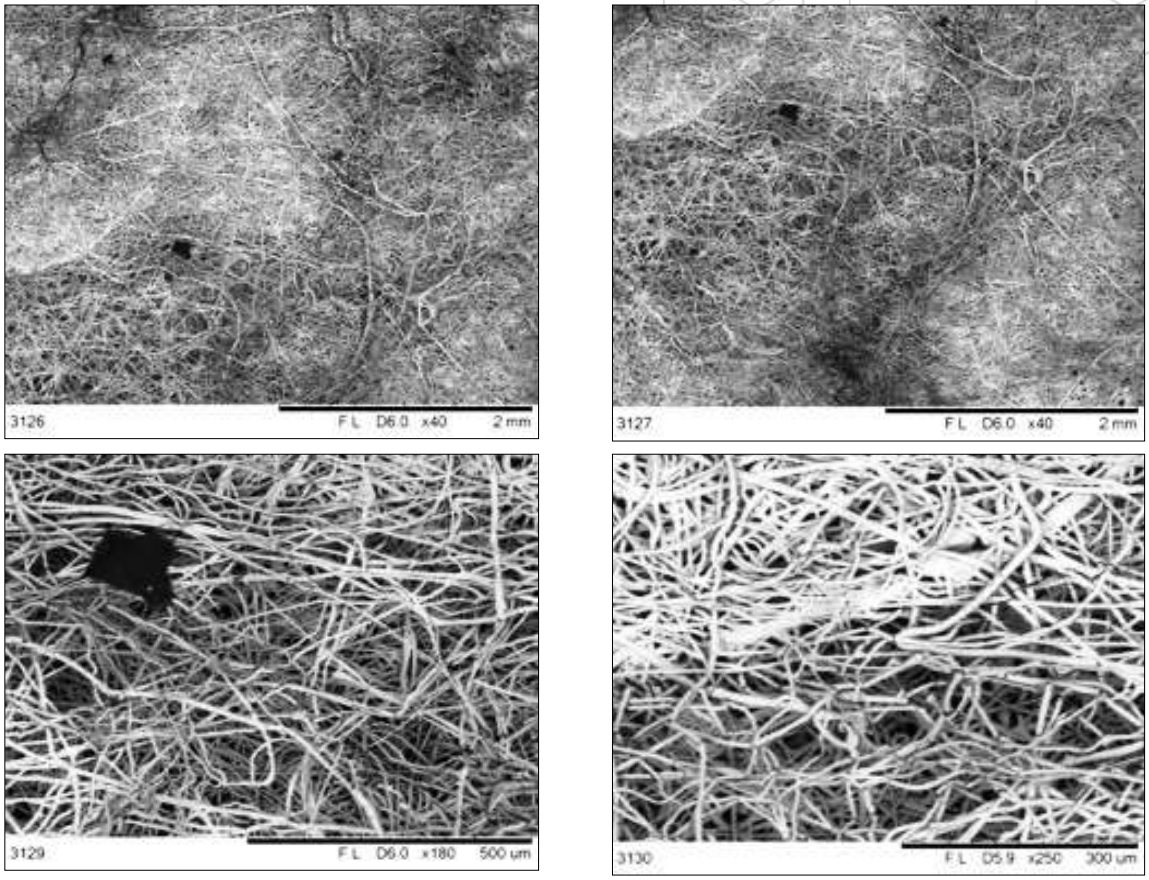

Figure 11. SEM images of the coPA veil' after metallization process.

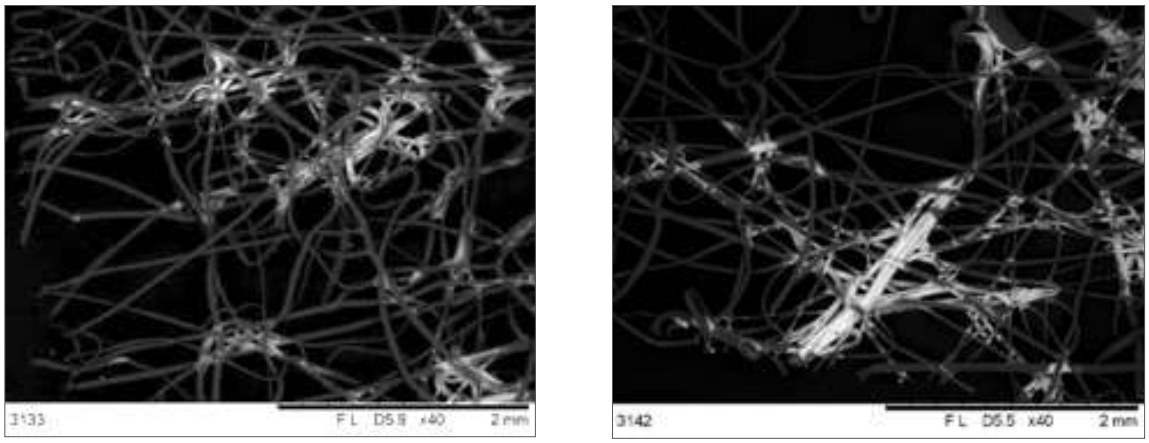

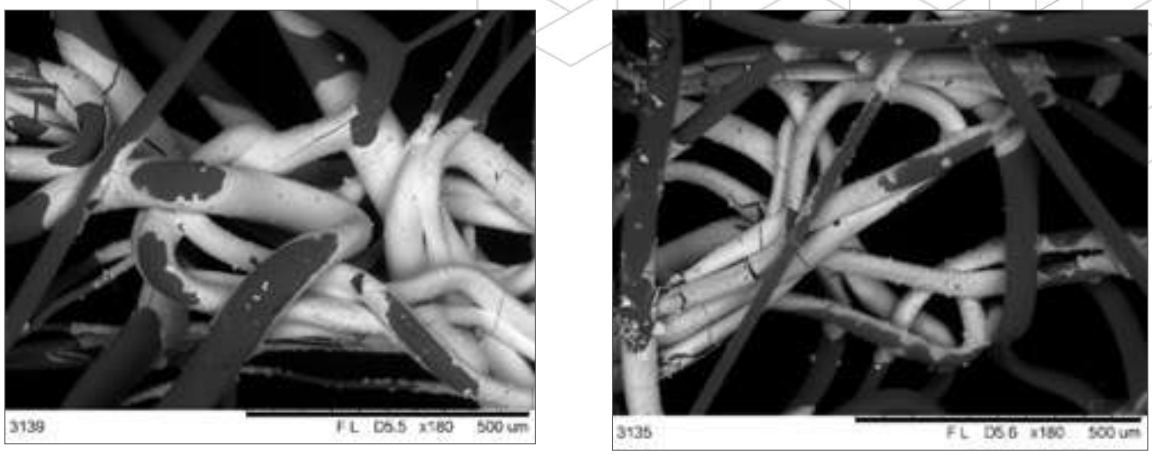

Figure 12. SEM images of the PPS+1wt% CNT veil' after metallization process.

The next trials were conducted only for PPS veils with 1wt% CNT and with two areal weight (25 and 60 g/m^2) on the longer step no7, which was extended to 20 minutes. The veils after metallization process are shown in Figure 4. It was observed that Ni-P layer is more stable and more durable that for the veils metallized at shorer time. The quality of the Ni-P layer was examined by SEM and the images are presented in Figure 5.

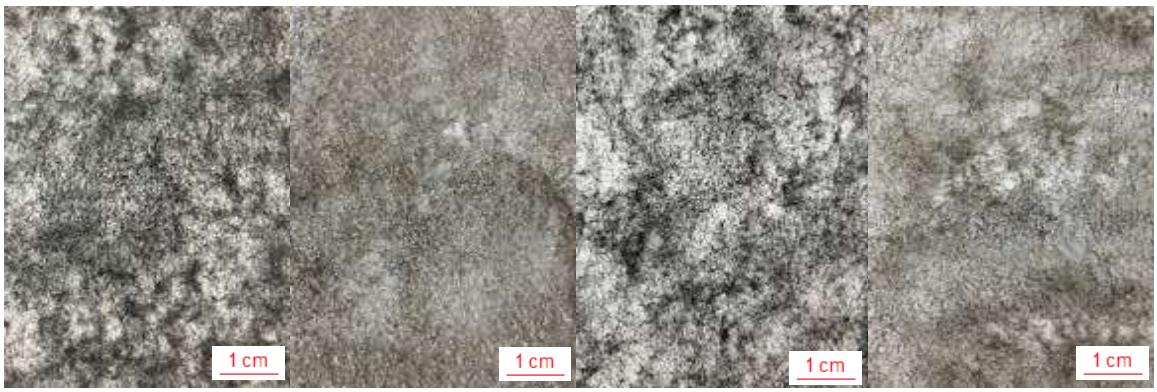

a) b) c) d)

Figure 13. Veil PPS+1wt% CNT 60gsm before (a) and after (b) metallization process. Veil PPS+1wt% CNT 25gsm before (a) and after (b) metallization process.

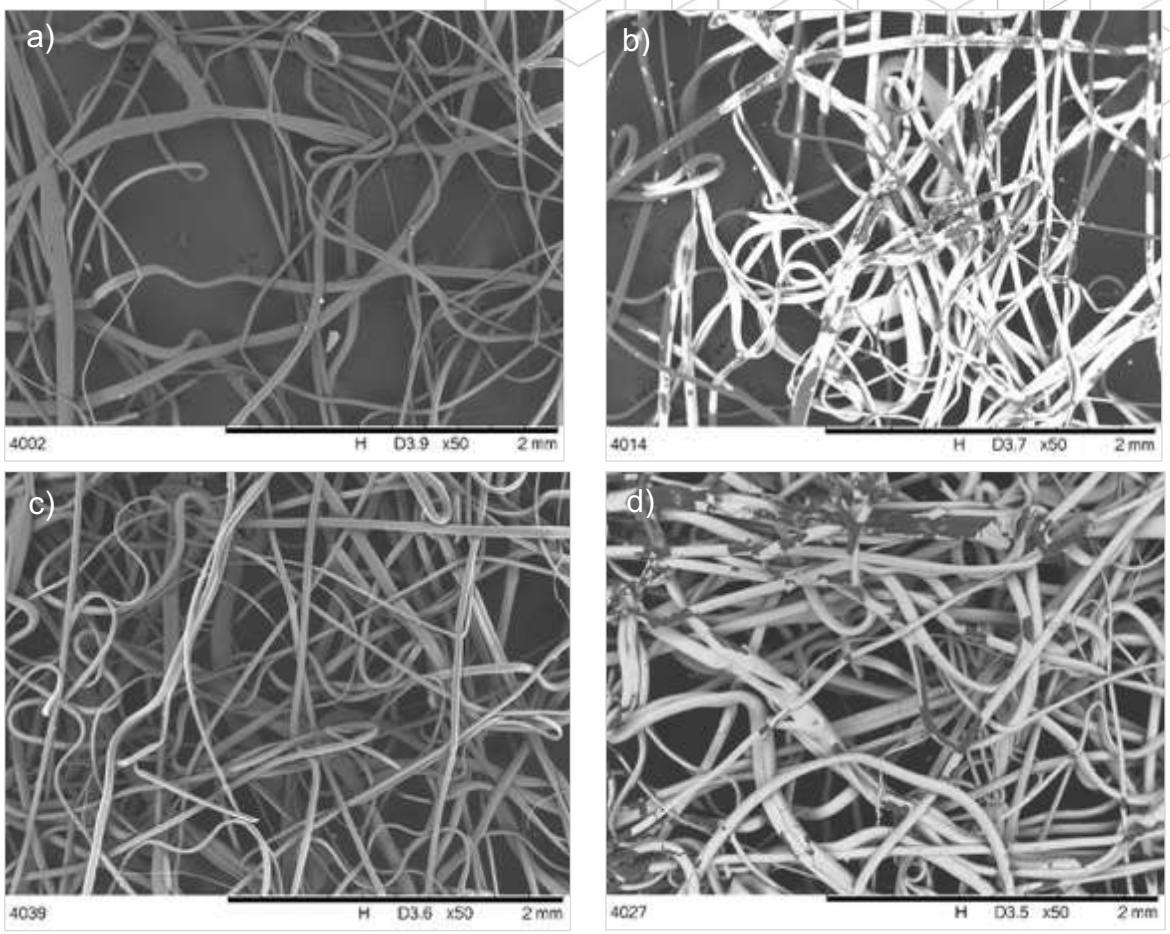

Figure 14. SEM images of veil PPS+1wt% CNT 60gsm before (a) and after (b) metallization process. Veil PPS+1wt% CNT 25gsm before (a) and after (b) metallization process.

Analysing the electrical conductivity of metallized veils (AFIT)

In particular research in Task 3 was focused on characterization of metalized veils type material for potential application in Structural Health Monitoring (SHM). Two types of initial characterization was performed: DC electrical characteristics and ability to generate heat with use of the material. For electrical characterisation purposes current-voltage (I-V) characteristics were be determined using the measuring source. For the measurement Keithley 2614B precise sourcemeter was used (Figure 6).

Number of measurement channels	2
Output power	200 W
Voltage source range	5 µV ÷ 200 V
Current source range	2 pA ÷ 10 A
Voltage measurement range	100 nV ÷ 200 V
Current measurement range	100 fA ÷ 10 A
Voltage source accuracy	(0.02 % + 375 µV) ÷ (0.02 % + 50 mV)
Current source accuracy	(0.06 % + 100 pA) ÷ (0.5 % + 40 mA)
Voltage measurement accuracy	(0.015 % + 225 µV) ÷ (0.015 % + 50 mV)
Current measurement accuracy	(0.06 % + 100 pA) ÷ (0.4 % + 25 mA)
Communication interfaces	Control panel, USB, Ethernet

Figure 15. Measuring source Keithley 2614B and operational parameters of the Keysight E4980A LCR meter.

Measurements of I-V characteristics were carried out on in 4 repetitions in voltage function as a dual sweep in range from -20V to 20V with step 1000.251 mV. Measure parameters were: voltage, current, power and resistance with minimum range 100nA with usage one 4 wire measurement unit, i.e. wires used for voltage supply were separated from wires used for measurement (Figure 7). Two types of veils were tested: PPS+1wt% CNT 25 gsm and PPS+1wt% 60 gsm. Non-linear behaviour of metalized veils was observed, particularly for veil PPS+1wt% 60 gsm beyond -10V or +10V (Figure 9). In addition to electrical characterization also initial thermal tests of the material were conducted. Using metalized veils it was possible to obtain significant temperatures above 60°C with application of relatively low voltage (Figure 9).

Figure 16. Metallized PPS veils connected with measurement system

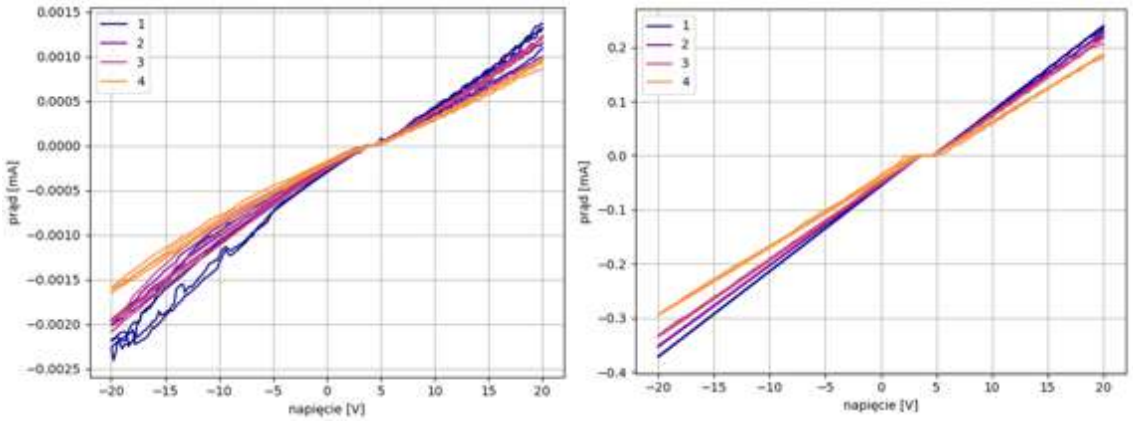

Figure 18. I-V characteristic of metallized veil PPS+1wt% CNT 60 gsm (right graphs) and veil PPS+1wt% CNT 25 gsm (right graph)

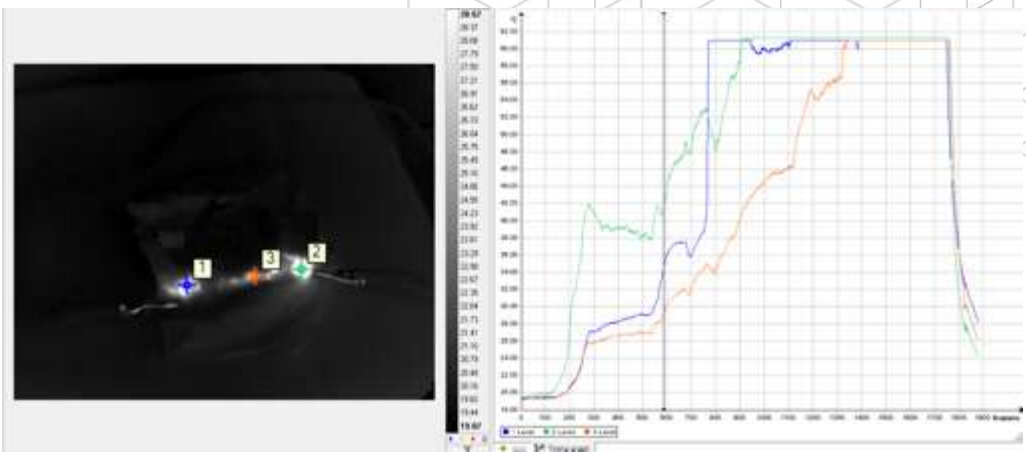

Figure 19. Thermogram and heating characteristic of metallized veils material.

Implementation of metallized veils into the GFRP structure (WUT)

The GFRP laminates were produced using HexPly® M9.6GF/32%/UD1200/G unidirectional epoxy-glass prepreg, where M9.6GF is the resin type; 32% is the resin content by weight; UD1200 means the fibers are arranged unidirectionally and the weight is 1200 g/m^2, and G indicates E glass fiber. M9.6GF can be used for the vacuum bagging process and is dedicated to large industrial parts and is also suitable for curing thin and thick sections. M9.6 GF exhibits long service life under ambient conditions. The vacuum bagging technique was utilized to produce GFRP composite laminates that contained nonmetallized, semi metallized and metallized nonwoven. The lay-up was created by successively stacking unidirectional epoxy-glass prepreg layers (HexPly® M9.6GF/32%/UD1200/G) and a nonwoven mat inside the laminate structure between -45^0 and 0^0 (Figure 10).

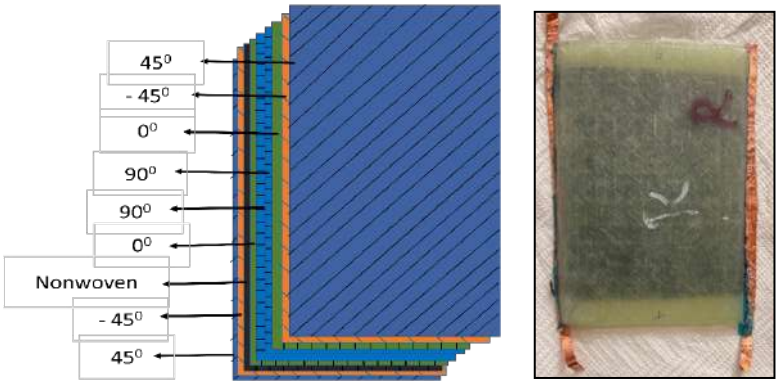

Figure 20. Lay-up sequence of composite prepreg and metallized nonwovens and ready GFRP panel for the measurement

The morphology of the GFRP laminate were analyzed by SEM and the images are presented in Figure 15. It is seen that the quality of the composite is good and the veils were melted creating the round shape islands in one of the layer.

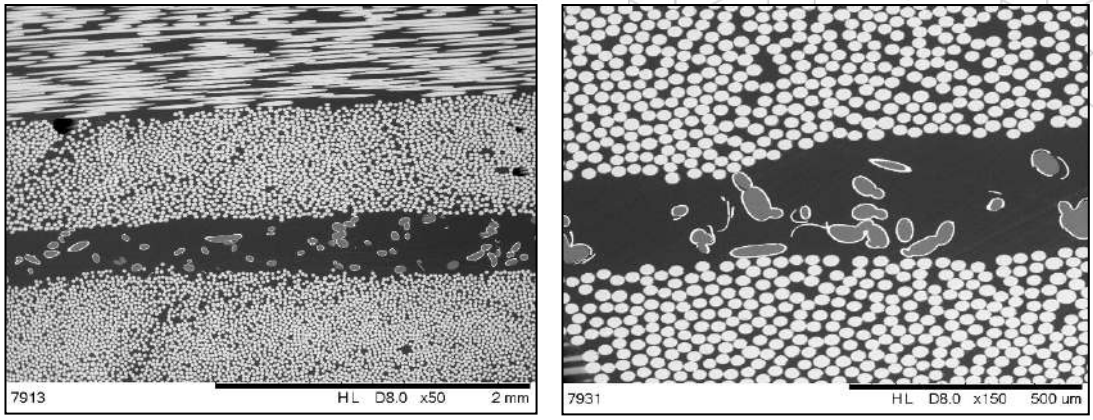

Figure 21. Cross-section of the GFRP panel with inserted metallized PPS veil.

Impact resistance test and active tomography (AFIT)

Impact resistance of the fabricated GFRP composites in accordance with ASTM D7136/D7136M standard. The tests utilized a drop-weight impact stand with a guided impactor to achieve exact vertical drop alignment. Laminates were rigidly clamped on all edges in the fixture to prevent movement during testing. The impact energy was 30 J, and the impactor weighed 5.526 kg. A hemispherical impactor was released from a predetermined height to deliver the desired impact energy. The specimens underwent testing before visual examination to determine the extent of damage zone size and nature followed by non-destructive inspection to evaluate delamination. All tests were performed at room temperature under controlled laboratory conditions. Figure 16, show the GFRP panel after impact test.

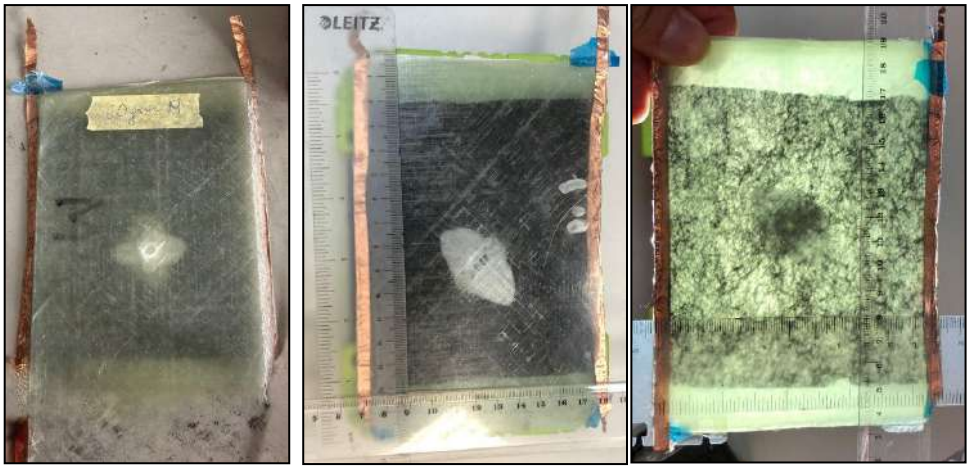

Figure 22. GFRP panel after impact test: front view, back view, back view with background light.

Active thermography was employed as a non-destructive testing (NDT) technique to detect and assess subsurface damage, delamination, in the fabricated GFRP. The FLIR SC7500 infrared camera recorded the surface temperature field of the sample through active thermography with its 320 × 256 pixel resolution and 10 frames per second frame rate and 1.5 to 5.1 µm spectral band. A high-voltage power supply AU-15P40 was used to generate thermal energy from metallized PPS+1wt% MWCNT nonwovens inside the

GFRP laminates. All analyzed samples were heated until a minimum temperature of 35^0C was recorded on the surface of the GFRPs.

An infrared camera placed directly above the heat source monitored the surface temperature changes from heating through to cooling down. The thermal image sequences underwent analysis through specialized software to produce thermograms and temporal contrast curves. The analysis showed subsurface defects consisting of delamination and resin-rich zones which appeared as areas with different cooling rates than the surrounding undamaged material. All tests were carried out at room temperature under stable ambient lighting conditions to minimize external thermal noise. The setup of the camera and the samples is shown in Figure 17.

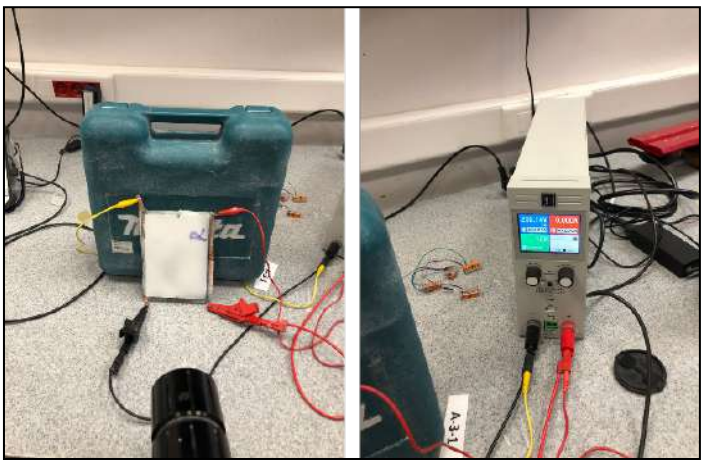

Figure 23. Setup of the camera and the GFRP panel

For the GFRP composites containing metallized veils, before impact (Figure 18A), the thermograms display several localized hot spots, corresponding to regions where heat is trapped by underlying defects. Compared to the metallized nonwoven, the overall thermal contrast is less uniform, with certain regions showing stronger responses while others remain weak. This behaviour can be attributed to the discontinuous metallization, which causes variations in surface conductivity and limits the redistribution of heat. After impact (Figure 18D), the number and intensity of visible hot spots increase, indicating that the impact loading introduces new damage sites and exacerbates pre-existing defects. However, the thermal contrast between defective and sound regions remains less homogeneous than in the metallized composite, confirming that the semimetallized structure provides lower heat-spreading efficiency. The temperature-time plots for the selected defect sites are shown in Figure 18B and 18E. Before impact, the highest defect response reaches around 43°C, while other sites display lower peaks in the range of 25-30 °C. Following impact, the maximum defect response increases to ~51 °C, accompanied by elevated peaks for the other defects as well. The cooling phase becomes more gradual after impact, reflecting a reduction in effective thermal diffusivity caused by delamination and microcracking. Compared to the metallized system, the composite with semimetallized nonwoven exhibits overall lower peak responses and less steep contrast among defect sites, reinforcing the idea that discontinuous metallization reduces the thermal amplification effect. The thermograms with marked defect sites (Figure 18C and 18F) demonstrate how partial metallization affects defect detection. Before impact (Figure 18C), four defects are visible, but their intensity levels differ significantly, with some being more clearly defined than others. After impact (Figure 18F), all defects remain identifiable, with sharper thermal contrast and enlarged hot spot areas, consistent with the progression of impact-induced damage.

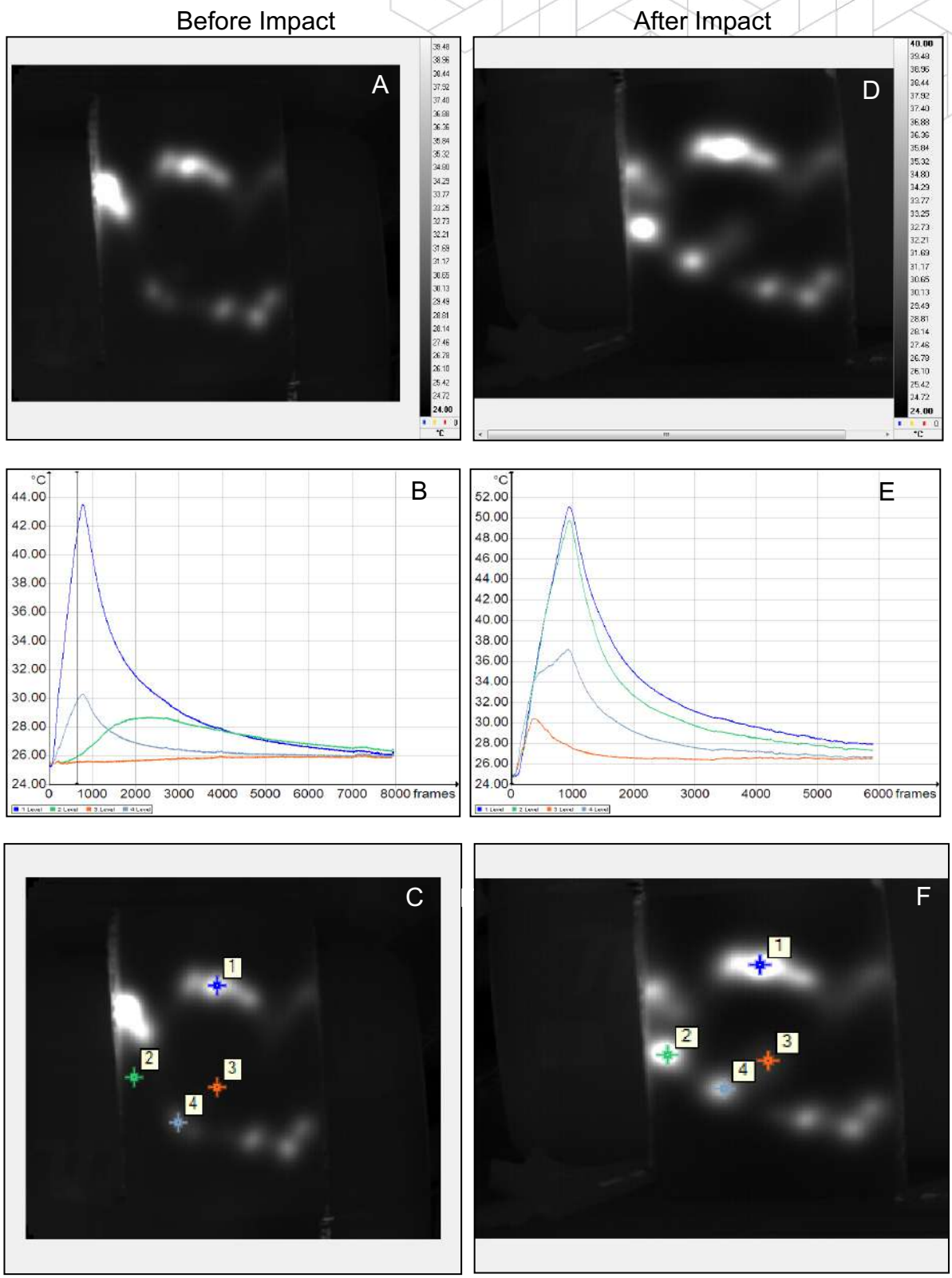

Figure 24. Images from active tomography test of GFRP before and after impact: thermograms (A,D), temperature distribution (B,E), thermograms showing the location of defects (C,F)

Conclusions

Based on the research, the overall, these findings indicate that the metallized CNT-doped veils reinforcements provide not sufficient enhancement in thermographic defect detection. Metallized PPS/1% MWCNT veils posses not homogenous NI-P layer that might disrupt the formation of continuous conductive network across the nonwoven structure. As a result, the metallized nonwoven cannot efficiently absorb or dissipate the thermal excitation (from an external heat pulse or electrical current) used in active thermography. The nonwoven material functions as an insulating layer when it lacks a conductive pathway because the heat flow remains weak and scattered which prevents the infrared camera from detecting any thermal contrast.

TASK 4 - INTEGRATION OF PZT SENSORS (LEADER: AFIT)

Due to diversity of PZT sensor technologies, they were applied in many areas, e.g.: precise control systems like modern fuel injection common rail, nano-opitcs, in dumping and control vibration system and energy harvesting. The inertia of piezoelectric transducers is very low, what is reason of using them in SHM systems as actuators and transducer for activating and receiving mechanical high frequency waves, transducers of mechanical vibration or strain gauges in fast processes, as well as accelerometers.

Importantly, piezoelectric transducers attached to a host structure can actuate and receive elastic guided waves. Application of elastic waves is one of the most universal approach to non-destructive testing of materials [1]. For excitation and detection of elastic waves, materials which exhibit piezoelectric properties need to be used [3]. Commonly applied as elastic waves actuators and sensors are transducers based on lead-zirconate-titanate (PZT) ceramics, i.e., PZT transducers [4][5]. Also, for over two decades now, PZT transducers have been applied to Structural Health Monitoring [6][7][8]. Elastic waves can interact with damages of different types[9], also they can propagate over long distances from their source, e.g., a PZT actuator. Therefore, sparse networks of PZT transducers can be used for monitoring relatively large structures, independently of the material used for manufacturing the structure. Due to those properties, PZT transducers have found a variety of applications in SHM. They can be applied to:

- fatigue crack and corrosion detection [10]-[15];
- bolt and bolted joint monitoring [16][17];
- adhesive and welded joint monitoring [18]-[22];
- detection of impact damage of composite materials [23]-[25]
- civil structure monitoring [26]-[28][30];
- transducers' self-diagnosis [21].

The application of PZT sensors to SHM is always based on the propagation of elastic waves, usually Lamb waves, through a monitored structure. One of the factors which can influence efficiency of PZT sensors in damage detection is technology of sensors integration with the monitored structure. For metallic or retrofited structures PZT sensors can be only attached to monitored surface with use of appropriate adhesives. In case of composite structures more options are available which are schematically presented in Figures below:

- surface attachment of PZT sensors (Figure);
- embedding of PZT sensors in additional technological layer of composite structure which is processed and cured in the same manufacturing process as the structure itself (Figure);
- embedding of PZT sensors into internal composite structure (Figure 27).

Advantages and disadvantages of particular methods of sensors integration with composite structure are briefly summarized in Table 1.

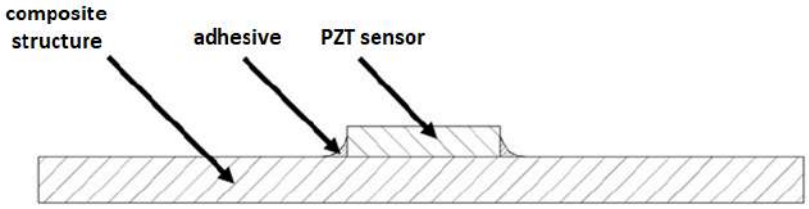

Figure 25: Cross section visualization of structure with surface attached PZT sensor

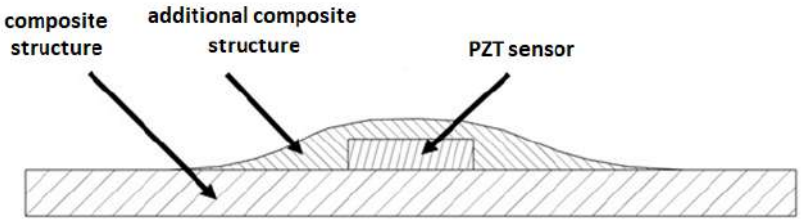

Figure 26: Cross section visualization of structure with PZT sensor embedded in additional layer of composite structure

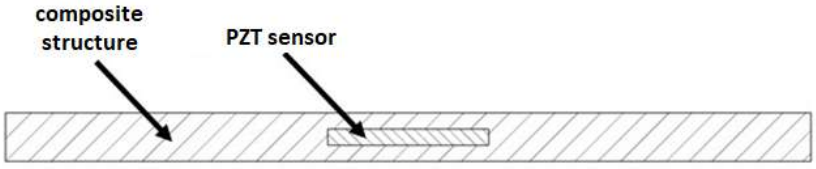

Figure 27: Cross section visualization of structure with PZT sensor embedded internally into composite structure

Integration method	Advantages	Disadvantages
Surface attachment	• the lowest costs of sensors installation, installation doesn't affect manufacture procedures and can be done after manufacturing is completed; • integration of sensors doesn't affect material properties of composite (in terms of strength, durability etc.) • in general, sensors can be replaced during maintenance if their performance decreased due to damage of ageing effects; • very small risk of sensors damage during installation; • no limitation on type and dimension of PZT sensors used;	• potentially the weakest acoustic coupling of PZT sensor with monitored structure which may result in amplitude of acquired signals and lower efficiency in damage detection or precision in damage localization; • surface attached sensors are the most vulnerable to damage during maintenance procedures; • potentially, influence of external conditions can be higher for surface attached sensors which may lead to higher risk of false positive indications; • potentially repeatability of sensors installation procedure might be low, therefore high variability of signal amplitude and damage detection

		efficiency between similar PZT networks installed on the same type of composite materials can occur;
Embedding in additional layer of composite material	• since sensors would be integrated with the structure in the same manufacturing process (curing etc.) as the host structure, acoustic coupling between sensor and material can be higher than in the case of surface attached sensors; • higher repeatability of sensors installation procedure (e.g. in terms of applied pressure, etc.) which can result in higher repeatability of system indication with respect to damage; • negligible influence on material performance (e.g. strength, durability, etc.) as sensors are included in local additional layer of composite material; • minimal impact on manufacturing process as sensors can be added after core material layup is finished, sensors connectivity quite straightforward; • additional layer provides some protection for sensors;	• potentially increased costs of sensors installation as manufacturing process of the composite needs to be adjusted; • limited possibility of sensors replacement as newly installed sensors wouldn't be integrated in the host structure in the same process, therefore acoustic coupling of replaced sensor can be different; • medium risk of sensors damage during installation; • some limitations on type and dimensions of PZT sensors used; • manufacturing process may have influence on properties of PZT sensors (due to temperature and pressure during the process);
Embedding in internal composite structure	• potentially the highest strength of acoustic coupling between sensor and composite material, therefore potentially the highest damage detection efficiency can be achieved; • sensors are protected from accidental during maintenance; • high repeatability of sensors installation procedure, therefore variability of SHM system indications should be lowest possible; • potentially, influence of some external conditions can be lower than for sesors installed on the surface;	• significantly increased costs of sensors installation as installation directly impact composite manufacturing process; • very complex methodology of sensors installation, proper technology for sensor connectivity must be developed; • high risk of sensors damage during installation process; • embedded sensors can influence mechanical properties of the material in terms of strength, durability, etc. • limited types of sensors can be used, as their dimensions (thickness in particular) needs to meet particular requirements; • manufacturing process may have influence on properties of PZT sensors (due to temperature and pressure during the process);

Table 1: Summary of sensors integration techniques

Capability 2 of the COMP-ECO project was focused on the investigation of different techniques of sensors integration with composite materials, in particular embedding of PZT sensors, encapsulated in veils, into the composite structure.

Based in recognized capabilities of COMP-ECO partners, the following research areas was followed in order to investigate benefits and disadvantages of different methodologies of sensors integration with the structure:

- Area 1: investigation of elastic waves interaction phenomena with real damage of composite material and development of appropriate signal processing methods for damage detection;
- Area 2: development of signal processing methods for external measurement conditions compensation;

Below short description of potential research activities in each area is presented.

Area no. 1:

Interaction of elastic waves with real damage is a complex phenomenon, especially for composite structures, e.g. for Barely Visible Impact Damage which can form transverse cracks of layers and multiple subsurface delaminations in the material.

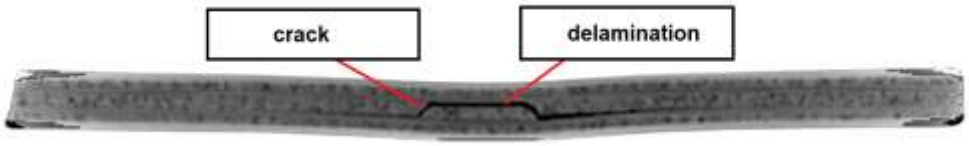

Figure 28: Cross section visualization of an impact damage of composite structure obtained with use of computer tomography

By examination of elastic waves interaction with damage it was possible to design appropriate signal processing method tailored to detect particular effects of such phenomenon. Such data can be obtained by proper numerical modelling or by full field data acquisition. ITWL as well as TU DELFT is equipped with Polytec PSV-500 laser scanning vibration measurement system (**Error! Reference source not found.**), which provided non contact signal acquisition along predefined network of scanning points, in case of TU DELFT system full out of plane and in plane decomposition of elastic waves is possible. Based on full information about distribution of guided waves scattering on damage, it is possible to verify different type of interaction phenomena between elastic wave and damage and determine the best type of signal characteristics useful for damage related signal changes detection. Also, by measurements acquired for pristine state of the structure and after damage introduction it is possible to assess efficient range of different signal characteristics for damage detection, which can provide a tool for proper PZT network configuration. During the project interaction of elastic waves with real damage, e.g. Barely Visible Impact Damage was examined, based on full field data acquisition with Polytec PSV-500 3D laser vibrometer which can provide non-contact signal acquisition along predefined network of scanning points. Series of tests were executed during research visit of AFIT researchers at TU Delft, with use of specimens manufactured by research team of WUT, AFIT and TPF at TU Dresden which demonstrated possibility of efficient research cooperation between partners of the project consortium

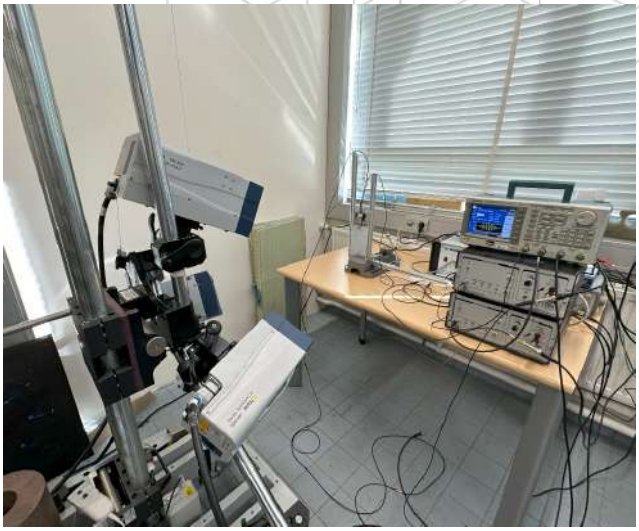

Figure 29: Laser vibrometer setup for 3D measurements of guided waves – tests of GFRP specimen equipped with PZT sensors during research visit of AFIT at TU Delft

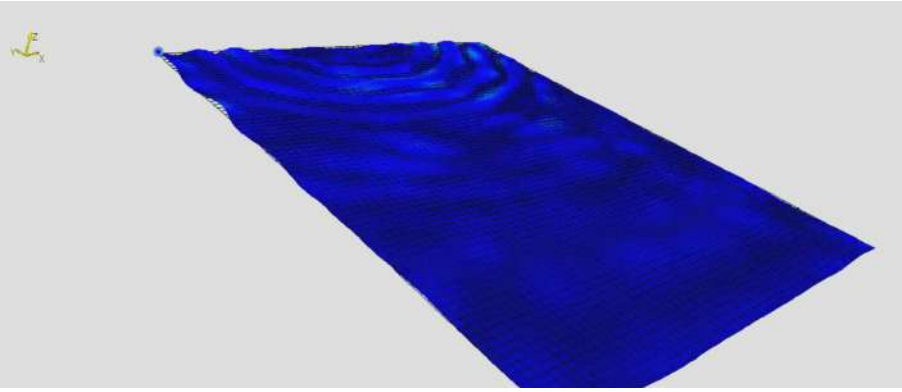

Figure 30. Snapshot of full field of guided waves distribution measured with use of 3D laser scanning vibrometer – obtained during research visit of AFIT at TU Delft

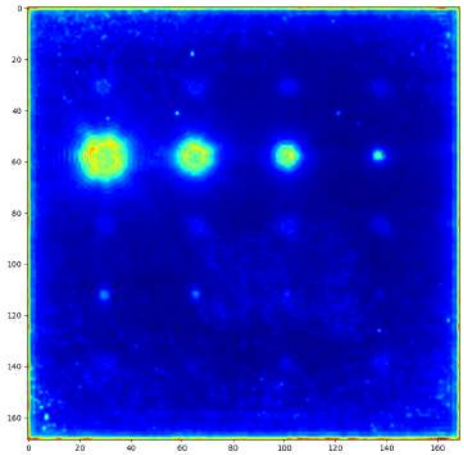

Figure 31 An example of damage detection visualization based on measurements with use of laser scanning vibrometer and appropriate signal processing

Specifically, within this subtask, we aimed to investigate the non-linear effects of elastic wave interactions with intra- and interlaminar cracks and delaminations in composite structures caused by impact damage. The main focus of activities was on examining the higher-order harmonics generation and frequency mixing resulting from microscopic damage but also on proper signal features definition, allowing for efficient damage characterization. Additionally, most efficient modes of elastic waves for detecting impact damage, both for embedded and surface-attached PZT sensors, were studied based on measurements with use of scanning laser vibrometer. Also, by measurements acquired for pristine state of the structure and after damage introduction it is possible to assess efficient range of different signal characteristics for damage detection, which can provide a tool for proper PZT network configuration (Figure). These properties can be determined for encapsulated PZT network embedded in the structure of composite and for surface attached sensor in order to better characterize different technologies of sensors integration. Efficiency characterization of surface attached and embedded PZT sensors extends current state of the art regarding application of PZT sensors.

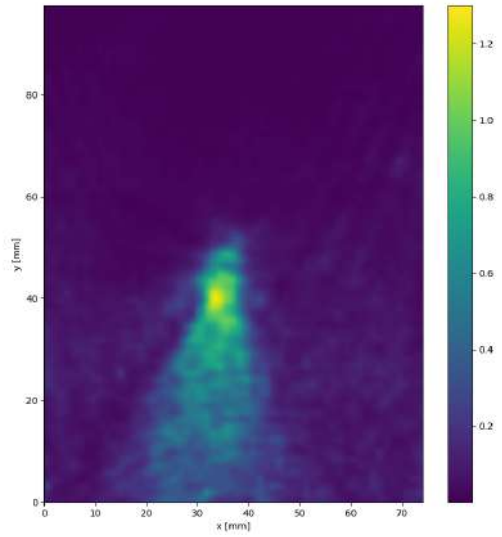

Figure 32 An example of correlation map for signals acquired with use of 3D laser vibrometer before and after impact damage introduction

During the project a series of low energy impact tests were conducted. Based on the developed signal analysis methods and data acquired by laser scanning vibrometer it was possible to visualize areas corresponding to signal distortions due to impact damage. The results were compared with conventional ultrasonic non-destructive evaluation of barely visible impact damage (BVID). The damage mapping results were in good agreement as shown in Figure .

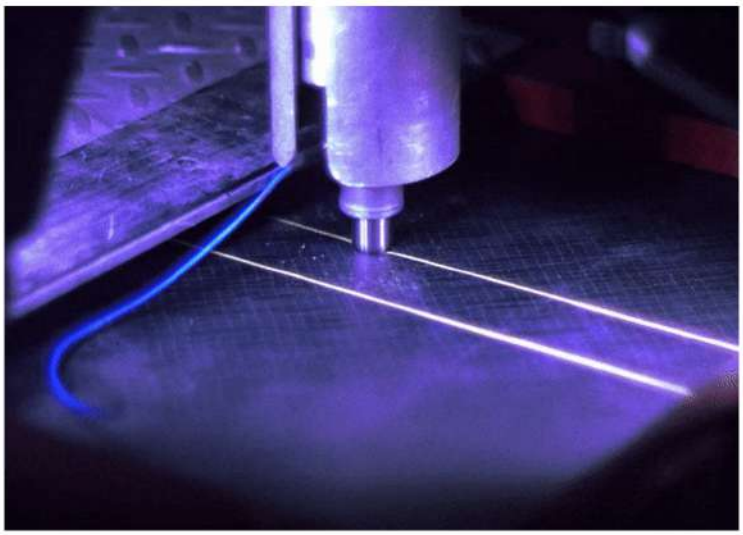

Figure 33 A snapshot obtained during low energy impact test of composite structures

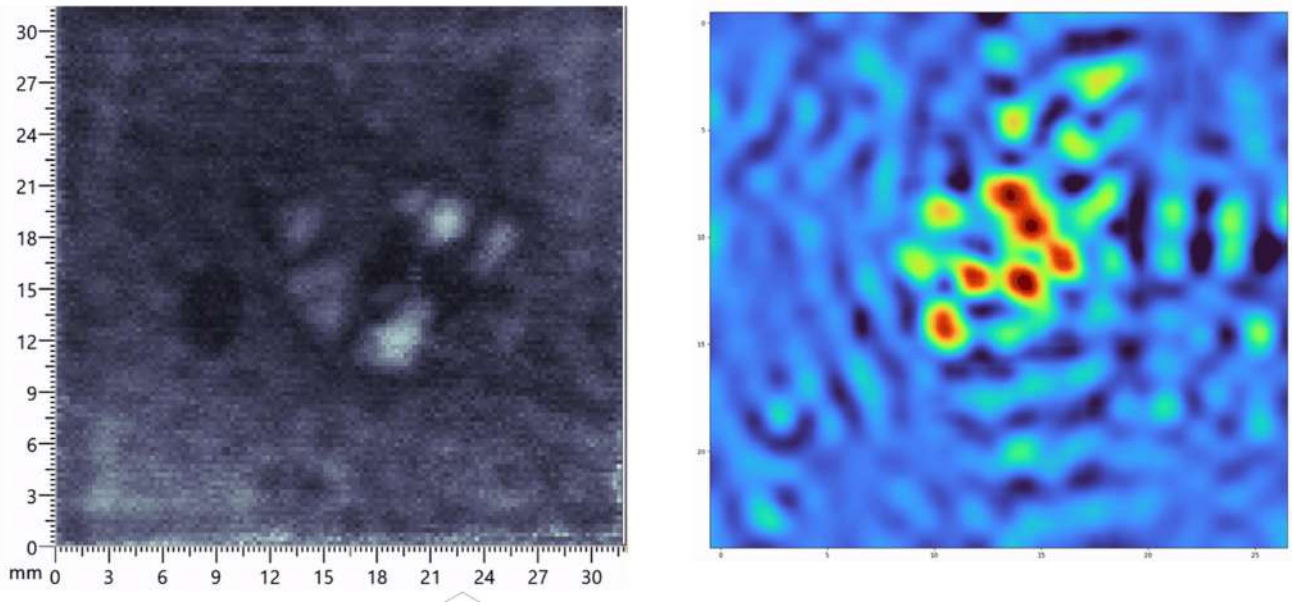

Figure 34 Comparison of damage evaluation by means of ultrasonic inspection (on the left) and with use of embedded PZT sensors and data obtained by laser scanning vibrometer (on the right)

During the project different sets of composite specimens, including embedded PZT sensors, were also prepared within the task.

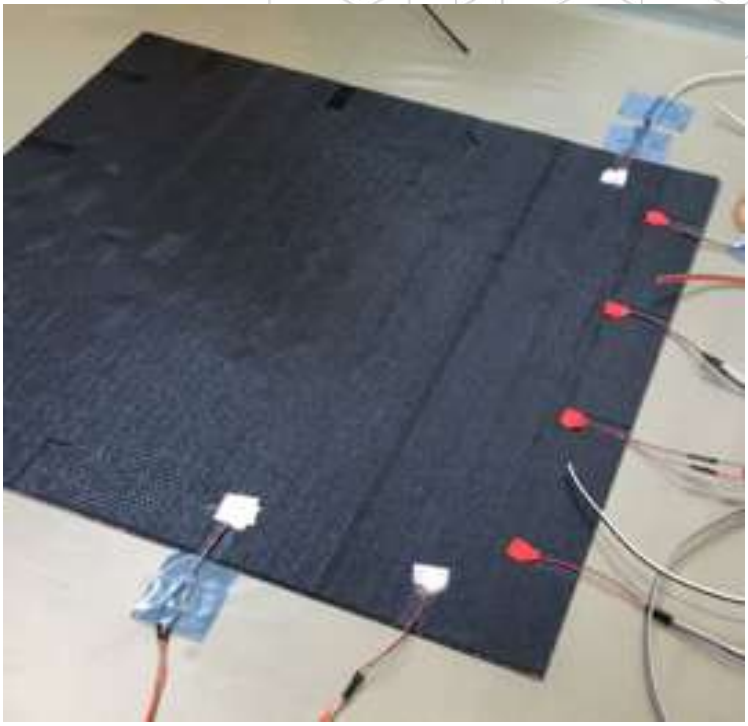

Figure 35 Specimen with embedded PZT sensors during preparation

Figure 36 Specimen with embedded PZT sensors after curing

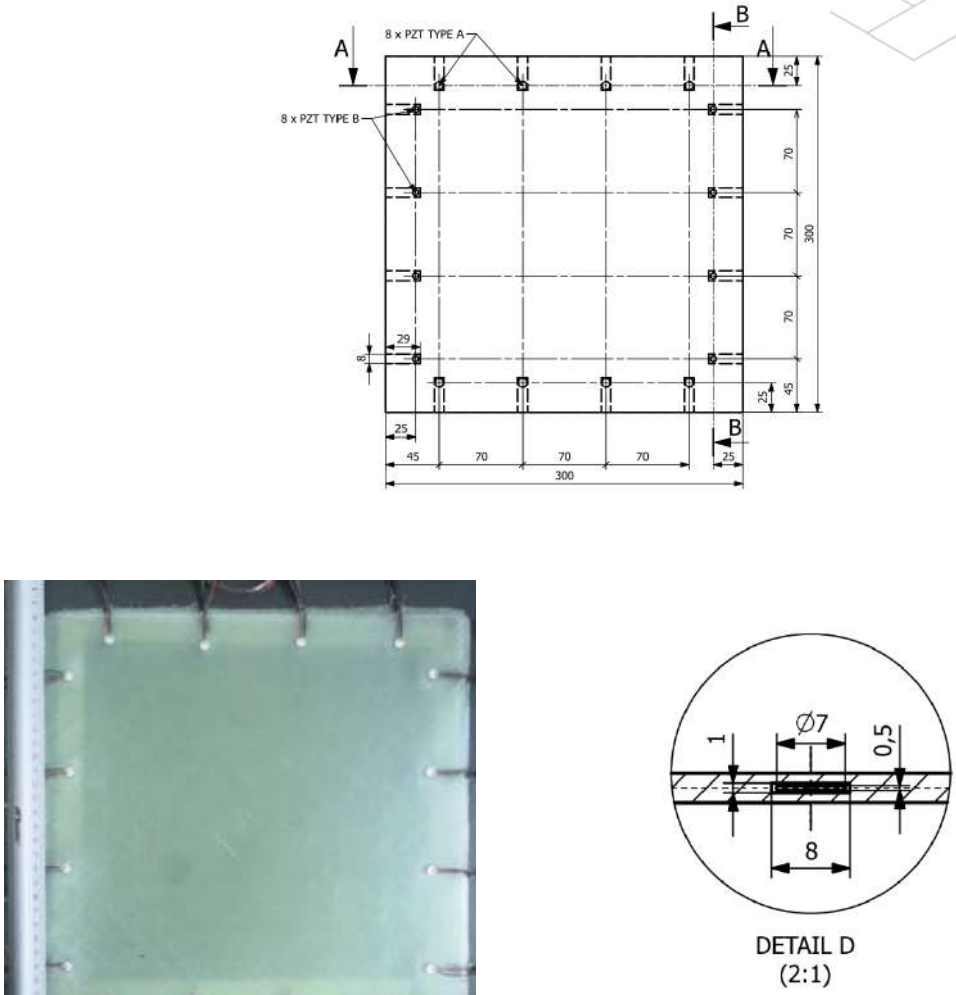

Figure 37: Scheme of a GFRP specimen with embedded embedded PZT sensors and view of specimen after curing

In addition, also investigation of non-linear effects on elastic waves propagation, which could be caused by intra- and interlaminar micro cracks and delaminations in composite structures was investigated within the task. The main mechanism under investigation involves higher-order harmonics generation and frequency mixing due to microscopic damage. Successful results of this area of research can lead to groundbreaking applications not only important for monitoring purposes of currently used composite structures, but also for early damage detection system important for safety of hydrogen storage tanks. In the project we used Finite element modelling (FEM) to investigate non-linear response of guided waves interacting with a single matrix crack. A 2 mm-thick unidirectional GFRP laminate with a single transverse matrix crack was established in ABAQUS, and the propagations of fundamental symmetric (S0) mode in the laminate were investigated. The influence of various crack lengths and depths on nonlinear guided waves were investigated. The results show that nonlinear responses happen when a crack exists and that the nonlinear responses differ with a half-thickness crack and through-thickness crack, which indicates the potential of using nonlinear guide waves to distinguish through-thickness crack from other crack scenarios in the composite laminate. The work has been presented during *The 2025 International Congress on Ultrasonics (ICU 2025)* and included in the conference proceddings:

- Tao, N., Dziendzikowski, M., Tao, R., Groves, R. M., & Yue, N. (2025). Numerical Study of Nonlinear Guided Waves in Composite Laminate with Matrix Crack. *Proceedings of the 2025 International Congress on Ultrasonics (ICU)*, 77. https://doi.org/10.5162/Ultrasonic2025/A8-b2

Also full open access article with detailed description of the obtained results was submitted to a relevant scientific Journal.

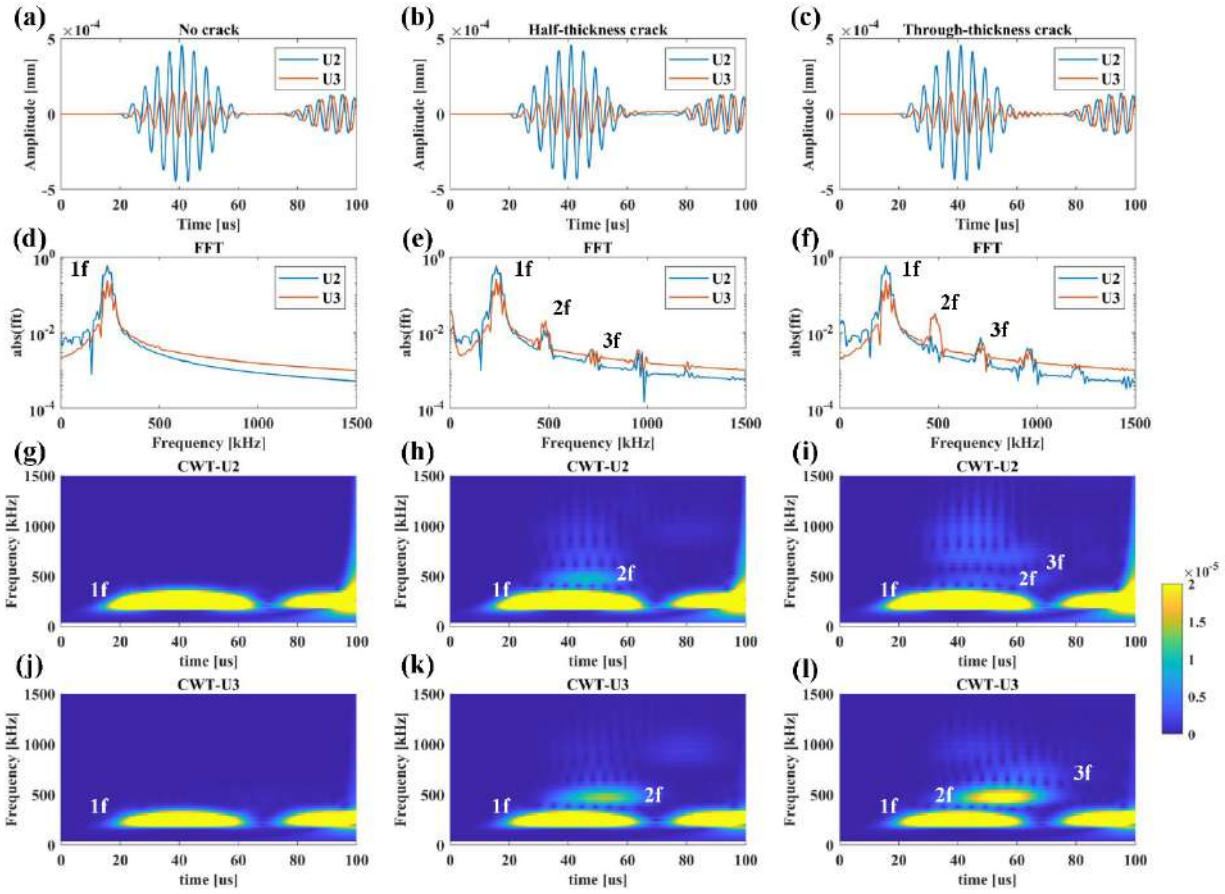

Figure 38: The amplitude, FFT, and CWT plots (U2 and U3) at the sensing position for no crack, half-thickness crack (crack depth 1 mm) and full-thickness crack (crack depth 2 mm) scenarios (crack length: 2 mm).

The predicted phenomena were evaluated experimentally. In Figure below, frequency spectrum of a guided waves signal before and after impact damage introduction is presented. It can be seen, that after damage introduction, the energy of the signal is redistributed, also, 1st order harmonics in the frequency range of 400 kHz (where 200 kHz was the excitation frequency) is apparent for the damaged structure. Non-linear signal features maps, such as redistribution of the signal energy between the excitation frequency and the 1st order harmonics as well as verification of signal linearity for the two excitation sources were also determined, visualizing impact damage resulting in forming delaminations and fiber cracking.

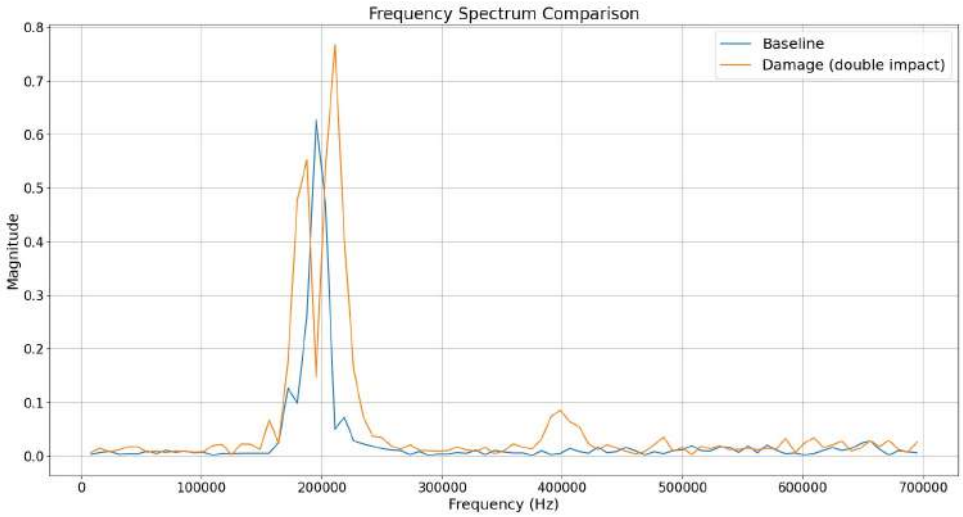

Figure 39: Frequency spectrum of guided waves propagation signal before and after damage introduction

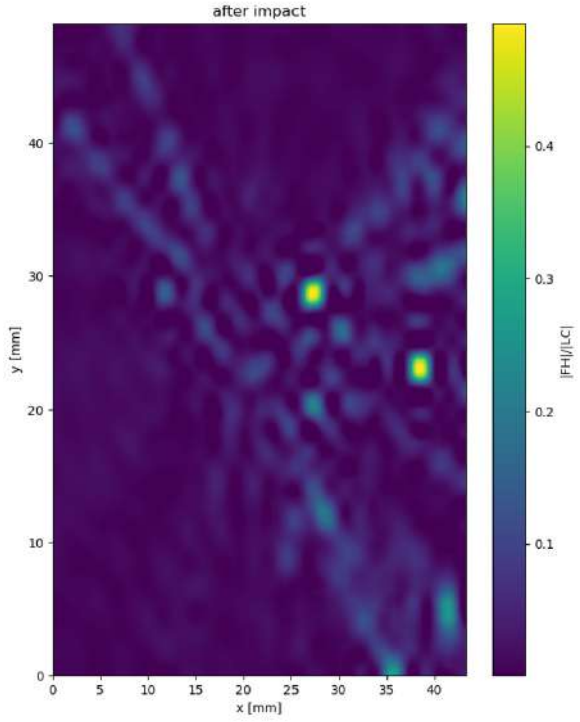

Figure 40: Mapping of non-linear signal feature after impact damage introduction

In addition to studies focused on development of proper techniques for signal analysis and damage characterization, also evaluation of different techniques for sensors integration was performed. In particular the following test were conducted in order to verify influence of sensors embedding technique on efficiency of composite structures monitoring with use of PZT sensors:

- cyclic loading – strain level corresponding to main landing gear attachment frame during landing, applied 100.000 cycles/landings;

- exposure to elevated temperature (70C) and high humidity (80%) for extended period of time (6 weeks) as well as to very low temperatures (below -70C).

Sensors maintained operational functionality after tests.

Figure 41: Chambers used for environmental tests

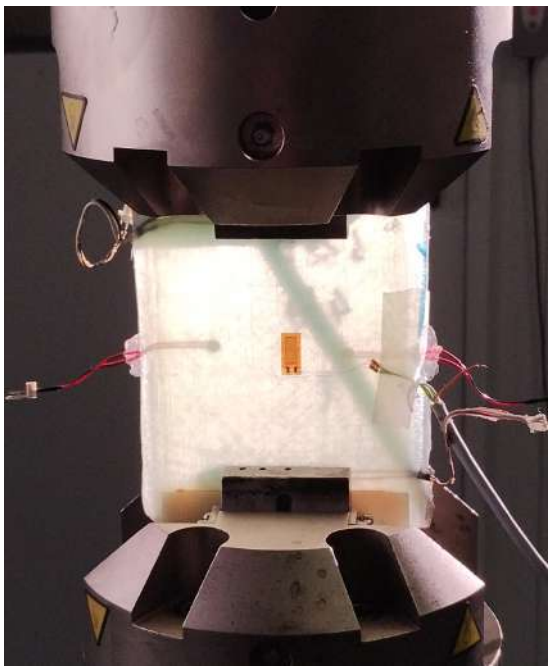

Figure 42: Composite structure with embedded PZT sensors during cyclic loading tests

Sensors sensitivity after cyclic loading and environmental exposure tests with respect to artificial damage with different damage diameters was evaluated. The best results were obtained for sensors embedded in the composite structure, however this technology of sensors integration are related to significant drawbacks related to complexity of specimens manufacturing and potential influence on mechanical properties of the specimen. Also, efficiency of sensors in detection of structure cracks due to overload during cycling loading was evaluated. In that case sensors embedded in additional technological layer on the surface of the composite structure as well as embedded in the structure revealed the highest sensivity to damage (Figure).

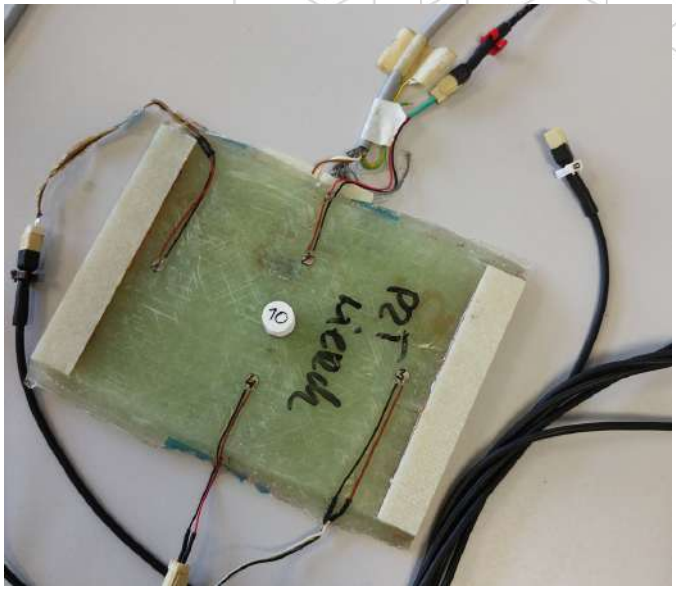

Figure 43: Test specimen with attached artificial damage

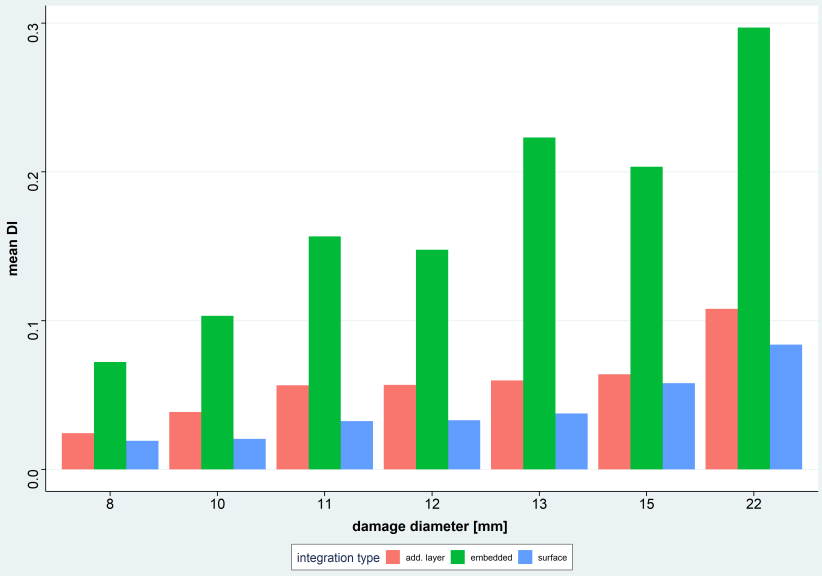

Figure 44: Comparison of PZT sensors sensitivity to artificial damage after cyclic loading test with respect to different techniques of sensors integration with the composite structure

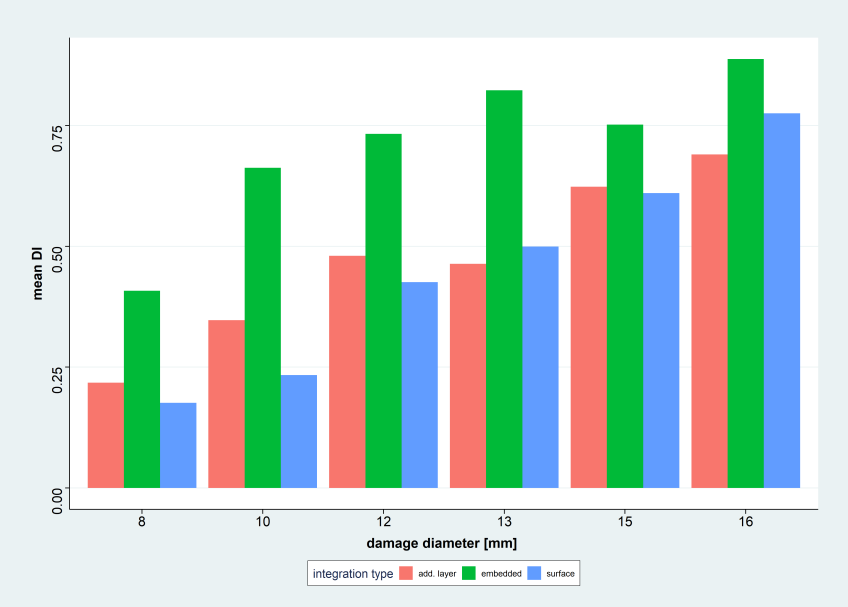

Figure 45: Comparison of PZT sensors sensitivity to artificial damage after environmental exposure test with respect to different techniques of sensors integration with the composite structure

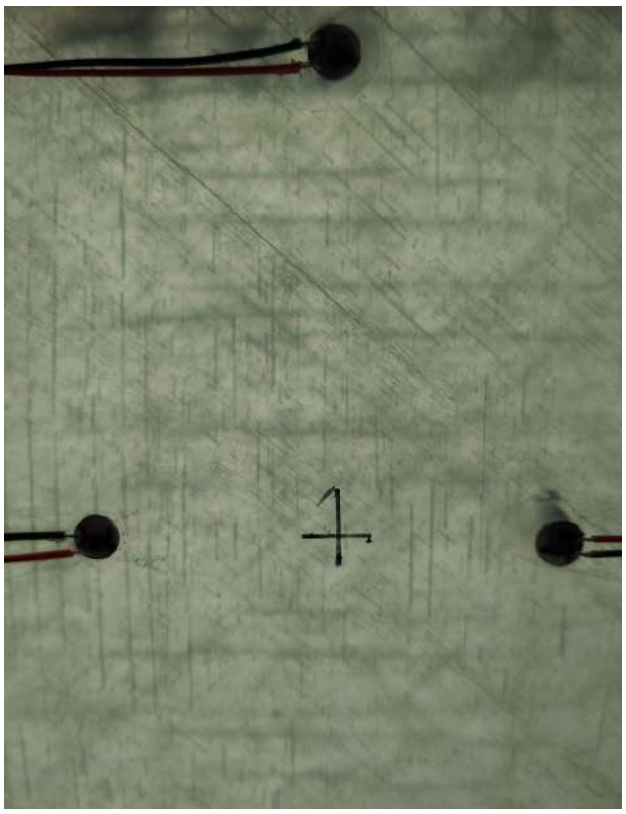

Figure 46: Cracks formed in the structure during cyclic loading of composite structures

Figure 47: Comparison of PZT sensors sensitivity to artificial damage after environmental exposure test with respect to different techniques of sensors integration with the composite structure

Summary

In the COMP-ECO project several results were obtained with respect to application of PZT sensors to composite structures monitoring and smart composite structures development were obtained. In particular non-linear effects of guided waves interaction with damage of the structure was examined, both experimentally as well as numerically. Also performance of different techniques of PZT sensors integration with the host structure was examined:

- surface attachment of PZT sensors;
- embedding of PZT sensors in additional technological layer of composite structure which is processed and cured in the same manufacturing process as the structure itself;
- embedding of PZT sensors into internal composite structure.

REFERENCES

[1] Vives, A. A. Piezoelectric transducers and applications. Springer, 2008.

[2] Davis, J.R. *ASM Handbook: Nondestructive Evaluation and Quality Control*; ASM International: Metals Park, OH, USA, 1989; Volume 17, ISBN 978-0-87170-023-0.

[3] Qin, Q.-H. *Advanced Mechanics of Piezoelectricity*; Springer: Berlin/Heidelberg, Germany, 2013; ISBN 978-3-642-29767-0.

[4] Ferrari, V.; Lucklum, R. Overview of acoustic-wave microsensors. *Piezoelectric Transducers and Applications*; Springer: Berlin/Heidelberg, Germany, 2008; pp. 39–62.

[5] Lim, Y.Y.; Kwong, K.Z.; Liew, W.Y.H.; Soh, C.K. Non-destructive concrete strength evaluation using smart piezoelectric transducer—A comparative study. *Smart Mater. Struct.* **2016**, *25*, 085021, doi:10.1088/0964-1726/25/8/085021.

[6] Su, Z.; Ye, L. *Identification of Damage Using Lamb Waves: From Fundamentals to Applications*; Springer: Berlin/Heidelberg, Germany, 2009; ISBN 0387848576.

[7] Giurgiutiu, V. *Structural Health Monitoring with Piezoelectric Wafer Active Sensors*, 2nd ed.; Academic Press: Tokyo, Japan, 2014; ISBN 0124186912.

[8] Staszewski, W.J.; Boller, C.; Tomlinson, G.R. *Health Monitoring of Aerospace Structures: Smart Sensor Technologies and Signal Processing*; John Wiley & Sons: Chichester, UK, 2004; ISBN 0470843403.

[9] Graff, K. *Wave Motion in Elastic Solids*; Oxford University Press: London, UK, 1975; ISBN 0486667456.

[10] Chan, H.; Masserey, B.; Fromme, P. High frequency guided ultrasonic waves for hidden fatigue crack growth monitoring in multi-layer model aerospace structures. *Smart Mater. Struct.* **2015**, *24*, 025037, doi:10.1088/0964-1726/24/2/ 025037.

[11] Giurgiutiu V.; Zagrai A. Damage Detection in Thin Plates and Aerospace Structures with the Electro-Mechanical Impedance Method. *Struct. Health Monit.* **2005**, *4*, 99–118, doi:10.1177/1475921705049752.

[12] Rabelo, D.S.; Steffen, V., Jr.; Finzi Neto, R.M.; Lacerda, H.B. Impedance-based structural health monitoring and statistical method for threshold-level determination applied to 2024-T3 aluminum panels under varying temperature. *Struct. Health Monit.* **2016**, *16*, 365–381, doi:10.1177/1475921716671038.

[13] Rao, J.; Ratasepp, M.; Lisevych, D.; Caffoor, M.H.; Fan, Z. On-Line Corrosion Monitoring of Plate Structures Based on Guided Wave Tomography Using Piezoelectric Sensors. *Sensors* **2017**, *17*, 2882, doi:10.3390/s17122882.

[14] Dragan, K.; Dziendzikowski, M. A method to compensate non-damage-related influences on Damage Indices used for pitch-catch scheme of piezoelectric transducer based Structural Health Monitoring. *Struct. Health Monit.* **2016**, *15*, 423–437, doi:10.1177/1475921716643492.

[15] Lim, Y.Y.; Soh, C.K. Electro-mechanical impedance (EMI)-based incipient crack monitoring and critical crack identification of beam structures. *Res. Nondestruct. Eval.* **2014**, *25*, 82–98, doi:10.1080/09349847.2013.848311.

[16] Ritdumrongkul, S.; Abe, M.; Fujino, Y.; Miyashita, T. Quantitative health monitoring of bolted joints using a piezoceramic actuator–sensor. *Smart Mater. Struct.* **2003**, *13*, 20, doi:10.1117/12.482381.

[17] An, Y.; Sohn, H. Integrated impedance and guided wave based damage detection. *Mech. Syst. Signal Process.* **2012**, *28*, 50–62, doi:10.1016/ j.ymssp.2011.01.016.

[18] Chiu, W.K.; Koh, Y.; Galea, S.; Rajic, N. Smart structure application in bonded repairs. *Compos. Struct.* **2000**, *50*, 433–444, doi:10.1016/S0263-8223(00)00110-0.

[19] Ochôa, P.; Villegas, I.F.; Groves, R.M.; Benedictus, R. Experimental assessment of the influence of welding process parameters on Lamb wave transmission across ultrasonically welded

thermoplastic composite joints. *Mech. Syst. Signal Process.* **2018**, *9*, 197–218, doi:10.1016/j.ymssp.2017.06.009.

[20] Roth, W.; Giurgiutiu, V. Structural health monitoring of an adhesive disbond through electromechanical impedance spectroscopy, *Int. J. Adhes. Adhes.* **2017**, *73*, 109–117, doi:10.1016/j.ijadhadh.2016.11.008.

[21] Dugnani, R.; Zhuang, Y.; Kopsaftopoulos, F.; Chang, F.-K. Adhesive bond-line degradation detection via a cross-correlation electromechanical impedance–based approach. *Struct. Health Monit.* **2016**, *15*, 650–667, doi:10.1177/1475921716655498.

[22] Zhuang, Y.; Kopsaftopoulos, F.; Dugnani, R.; Chang, F.-K. Integrity monitoring of adhesively bonded joints via an electromechanical impedance-based approach. *Struct. Health Monit.* **2017**, doi:10.1177/1475921717732331.

[23] Gresil, M.; Yu, L.; Giurgiutiu, V.; Sutton, M. Predictive modeling of electromechanical impedance spectroscopy for composite materials. *Struct. Health Monit.* **2012**, *11*, 671–683, doi:10.1177/1475921712451954.

[24] Dziendzikowski, M.; Kurnyta, A.; Dragan, K.; Klysz, S.; Leski, A. In situ Barely Visible Impact Damage detection and localization for composite structures using surface mounted and embedded PZT transducers: A comparative study. *Mech. Syst. Signal Process.* **2016**, *78*, 91–106, doi:10.1016/j.ymssp.2015.09.021

[25] Gao, W.; Wu, Z.; Yang, L.; Zheng, Y. Integrated impedance and Lamb wave–based structural health monitoring strategy for long-term cycle-loaded composite structure. *Struct. Health Monit.* **2017**, doi:10.1177/1475921717717312.

[26] Dixit, A.; Bhalla, S. Prognosis of fatigue and impact induced damage in concrete using embedded piezo-transducers. *Sens. Actuator A-Phys.* **2018**, *274*, 116–131, doi:10.1016/j.sna.2018.03.005.

[27] Ayres, J.W.; Lalande, F.; Chaudhry, Z.; Rogers, C.A. Qualitative impedance-based health monitoring of civil infrastructures. *Smart Mater. Struct.* **1998**, *7*, 599.

[28] Gu, H.; Moslehy, Y.; Sanders, D.; Song, G.; Mo, Y.L. Multi-functional smart aggregate-based structural health monitoring of circular reinforced concrete columns subjected to seismic excitations. *Smart Mater. Struct.* **2010**, *19*, 6, doi:10.1061/41096(366)272.

[29] Wang, D.; Song, H.; Zhu, H. Numerical and experimental studies on damage detection of a concrete beam based on PZT admittances and correlation coefficient. *Constr. Build. Mater.* **2013**, *49*, 564–574, doi:10.1016/j.conbuildmat.2013.08.074.

[30] Providakis, C.P.; Stefanaki, K.D.; Voutetaki, M.E.; Tsompanakis, J.; Stavroulaki, M.E. Damage Detection in Concrete Structures using a Simultaneously Activated Multi-mode PZT Active Sensing System: Numerical Modelling. *Struct. Infrastruct. Eng.* **2014**, *10*, 1451–1468, doi:10.1080/15732479.2013.831908.

[31] Dragan K.; Dziendzikowski M. A method to compensate non-damage-related influences on Damage Indices used for pitch-catch scheme of piezoelectric transducer based Structural Health Monitoring. *Structural Health Monitoring*, **2016**, 15(4), 423-437.

TASK 5 - INSULATION OF SENSORS (LEADER: WUT)

Research Task 5 concerns the development of an effective method for isolating PZT sensors and conductive fibers/strips using neat nonwovens. This is dictated by the use of sensors in a CFRP structure that are conductive, and it is necessary to provide a barrier between the sensor and the carbon fibres.

During an internship at TU Dresden, 2 sets of samples were produced: with CNT-doped strips and conductive paths (also with CNTs added), and neat PBT-based veils were used to verify isolation efficiency. The samples produced are presented in the images below.

The PBT-based nonwovens were manufactured and supplied by TPF, while the laminates were manufactured by WUT and TU Dresden.

Results:

When CNT-doped strips were used (Figure 1), an identical connection to the cables was made using conductive epoxy adhesive as in research task 2. It was observed that not all strips are well insulated. The reason was the use of epoxy glue that had not yet cured. Therefore, it is planned to perform this procedure in two steps - first, connect the cables with CNT-doped strips and epoxy adhesive (and wait for it to cure), and then introduce the sensors into the CFRP structure.

Figure 48. CFRP system with strips

Figure 49. CFRP system with conductive grids

In the case of laminates containing conductive grids, electrodes in the form of copper tapes were used - also as planned in Research Task 2. The shape of the electrode used at both ends of the laminate did not work well, as after the crosslinking process in the laminate, problems were encountered with the separation of the electrode from the carbon prepreg layers, and as a result, the inability to connect to a current source. Therefore, the next step is planned to use a different electrode shape and to protect the copper tape with a high-temperature film that would isolate it from the carbon prepreg layers. Only then will it be possible to verify the effectiveness of the insulation used.

During next stay at TU Dresden, 23 CFRP samples with different arrangements of neat veils were produced to verify the isolation efficiency. A part of the produced samples was characterized by effective isolation performance (Table 1), while the second presents systems for which the required level of isolation was not observed (Table 2).

Table 1. Proposed systems meeting the required insulation level

Working insulation								
Material	GSM [g/m2]	Numer of layers	Layout	Resistivity (50V)	Resistivity (250V)	Resistivity (1000V)	Resistance	Thickness [mm]
PA12	10gsm	12		>55M OM	>275M OM	>2,2G OM	Off the scale	1,26
PPS	35gsm	8		>55M OM	>275M OM	>2,2G OM	Off the scale	1,22
Breather PET	-	1		>55M OM	>275M OM	>2,2G OM	Off the scale	1,27
Breather PET	-	2		>55M OM	>275M OM	>2,2G OM	Off the scale	1,69
PBT	16gsm	6		>55M OM	>275M OM	>2,2G OM	Off the scale	1,31
PBT	16gsm	8		>55M OM	>275M OM	>2,2G OM	Off the scale	1,22
PBT	16gsm	8		>55M OM	>275M OM	>2,2G OM	Off the scale	1,22
PBT	16gsm	8		>55M OM	>275M OM	>2,2G OM	Off the scale	1,26
mix PBT(A) G1841(B)	A -16gsm B - 14gsm	A - 2 B - 2	A1/B1/B1/A1	>55M OM	>275M OM	>2,2G OM	Off the scale	1,18
mix PBT(A) G1841(B)	A -16gsm B - 14gsm	A - 3 B - 3	A1/B1/A1/B2/A1	>55M OM	>275M OM	>2,2G OM	Off the scale	1,25

Table 2. Proposed systems do not meet the required insulation level

Not working insulation								
Material	GSM [g/m2]	Numer of layers	Layout	Resistivity (50V)	Resistivity (250V)	Resistivity (1000V)	Resistance	Thickness [mm]
PA12	10gsm	4		0M OM	0M OM	0M OM	0,150k OM	1,15
PA12	10gsm	8		0M OM	0M OM	0M OM	0,310k OM	1,29
PPS	27gsm	2		0M OM	0M OM	0M OM	0,030k OM	1,13
PPS	27gsm	4		0M OM	0M OM	0M OM	0,040k OM	1,09
PPS	35gsm	2		0M OM	0M OM	0M OM	0,015k OM	1,13
PPS	35gsm	6		0M OM	0M OM	0M OM	0,130k OM	1,20
PBT	14gsm	4		0 MOM	0M OM	0M OM	0,125k OM	1,21
G1841	14gsm	4		0M OM	0M OM	0M OM	0,180k OM	1,14
G1841	14gsm	6		0M OM	0M OM	0M OM	0,220k OM	1,22
G1841	14gsm	8		0M OM	0M OM	0M OM	0,245k OM	1,22
G1841	14gsm	8		0M OM	0M OM	0M OM	3,6k OM	1,19
G1841	14gsm	8		0M OM	0M OM	0M OM	0,160k OM	1,17
mix PBT(A) G1841(B)	A -16gsm B - 14gsm	A - 4 B - 4	A2/B2/B2/A2	0M OM	0M OM	0M OM	0,180k OM	1,25

Conclusion:

As part of the work carried out in TASK 5, 8 effective systems were developed, allowing for complete isolation of sensors and, as a result, their application in CFRP laminates. From a

processing perspective, the most recommended configurations are: 8 layers of PBT (16 gsm) and 12 layers of PA12 (10 gsm).

TASK 6 - CONNECTION WIRES AND CONTACT POINTS (LEADER: AFIT)

The task was devoted to investigate alternative types of connections to replace the standard method of solder joints within the applications for temperature-sensitive materials as well as not suitable for soldering. Selected approaches of connecting and contacting e.g. CNT-based conductive elements with copper interconnection wires, based on the Consortium experience and state-of-the-art are taken under consideration:

a) bonding elements with conductive pastes;

b) direct, mechanical connection of CNT-doped strip with a copper wire, wrapped around the strip;

c) direct, crimped connection of CNT-doped fibers with a copper wire.

Table. Types of connections investigated

Type 1	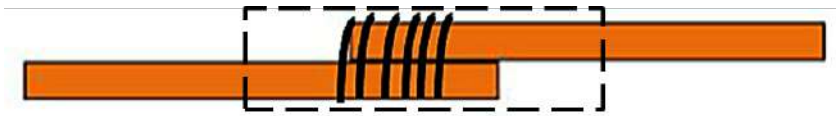	Stranded copper wire is lap-joint with a CNT strip with additional wire wrapping
Type 2	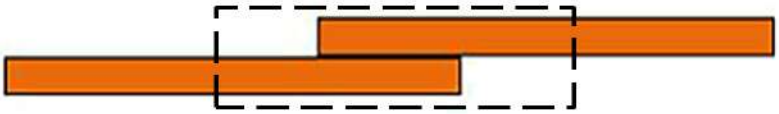	Stranded copper wire and CNT strip as a single lap-joint
Type 3	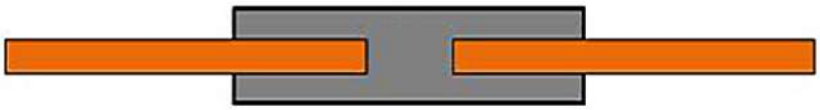	Stranded copper wire and CNT strip in a face-to-face connection in a crimped copper tube

Within electronics, the reliability of electrical interconnections between various conductive elements, sensors with the measuring and excitation equipment is crucial for the system performance and stability. Using a conductive adhesive with e.g. silver metallic particles to contact non-solderable materials is considered as a promising method, and is investigated within printed/ flexible/ organic electronics area.

Performed tensile tests of connections, prepared as shown in Table T6.1 with concurrent resistance measurements, revealed as follow:

- Type 3 connection (crimped in copper tube) has shown the highest tensile strength, reaching 30N ± 2N. Connections of type 2 and type 1 lost their conductivity at approx. 23 N and 18N respectively;

- The lowest initial contact resistance has been obtained for type 1 connection (wrapping), but type 3 also give satisfactory level of contact resistance below 20 mΩ;
- In all cases, prior atmospheric plasma treatment of the strip and wire in a contact area show slight increase in tensile strength, regardless the connection type;
- However, it was found that plasma treatment could lead to increased contact resistance for the same type of a connection.

Tensile tests (Figure T6.1) were performed during the internship at TU Dresden, where the concept and preparation of connection-test samples was conducted by AFIT, strips were manufactured by TPF, the test execution and data analysis was the joint co-operation of AFIT and TU Dresden.

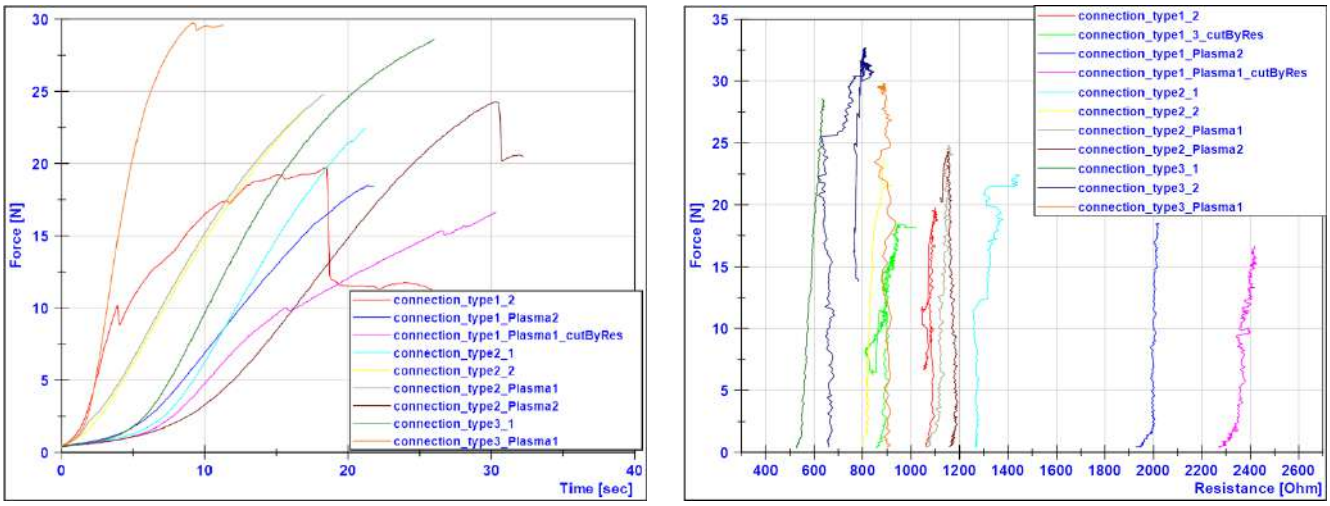

a) b)

Figure T6.1. Results of the tensile / resistance connection types tests, a) resilience by means of maximum force at breakage, b) test sample overall resistance change due to applied force

Based of tensile test of connections, taking into account the time-consuming nature and susceptibility to human error of making a type 3 connection, as well as considering the type 1 connection as comparable in strength, the optimization process was performed. Due to variety of conductive elements (strips, grids, printed strains sensor) to be embedded into prepared composite structures , a dedicated approach was used to make the connection with the measuring copper wire.

The adopted methodology to prepare connections assumes:

- for connecting strips and fibers with copper wire – wire wrapping was used with additional layer of conductive adhesive, to decrease contact resistance. The connection was pre-cured, before placing the circuit in the composite structure.

  Strips and fibers based circuit were used e.g. as a heater embedded into GRFP, to detect impact damage.

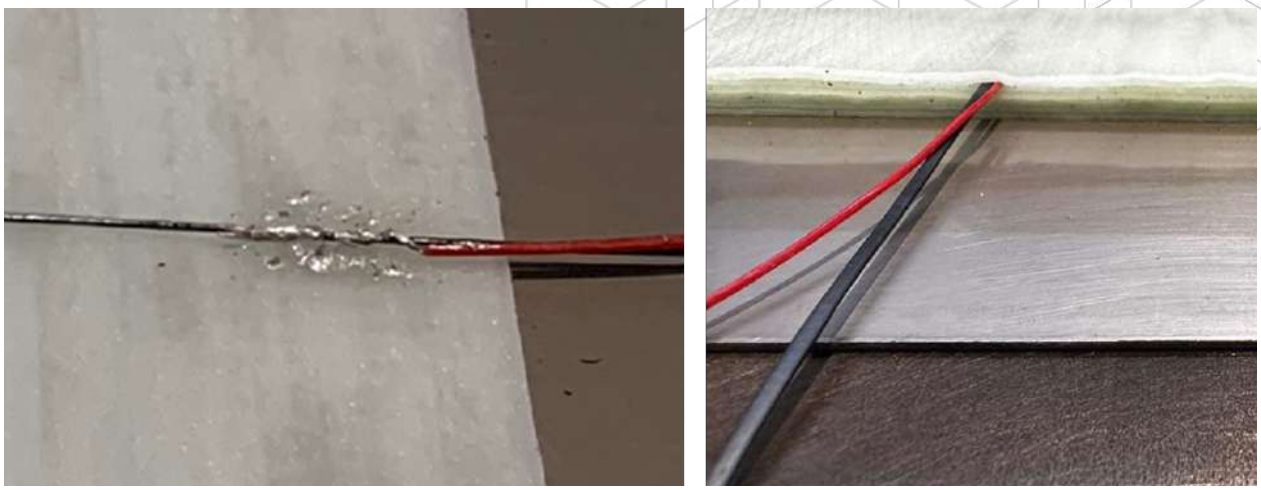

Figure 51. Connection for CNT stips and fibers

- for connecting CNT-based Strain Sensors - fabricated using FDM printed from a copolyester base material filled with MWCNT on a integrated a non-woven substrate. Those sensors were embedded into the composite, and in collaboration with AFIT, a method was developed for extending connections beyond the composite structure. In that case, sensor – copper wire connection was performed as a lap-joint of CNT material and copper sheet with intermediate layer of conductive adhesive. Based on investigation, this method ensures that the electric connection joints maintained its conductivity in the autoclave process.

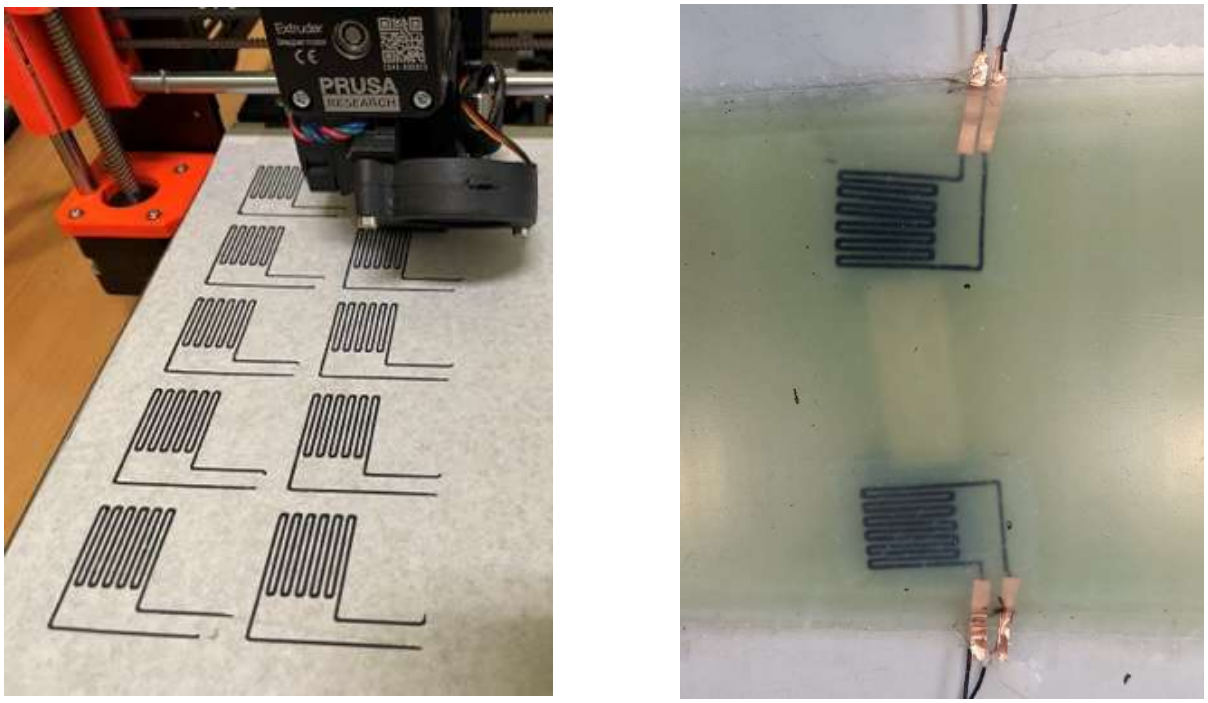

a) b)

Figure 52 CNT-based Strain sensor a) manufacturing, b) integrated into GRFP elementwith copper connectors

- for connecting CNT-based conductive grids – CNT-based thermoplastic meshes were produced and supplied by TFP, a connection methodology to excitation wires was joinly developed in collaboration with AFIT, and is similar to CNT-based strain sensors. Side-grid copper tape electrodes with intermediate conductive adhesive layer was cured within the same process as GRFP composite element. After autoclave process, copper tape electrode was used to solder excitation wire and maintaining electrical connection continuity.

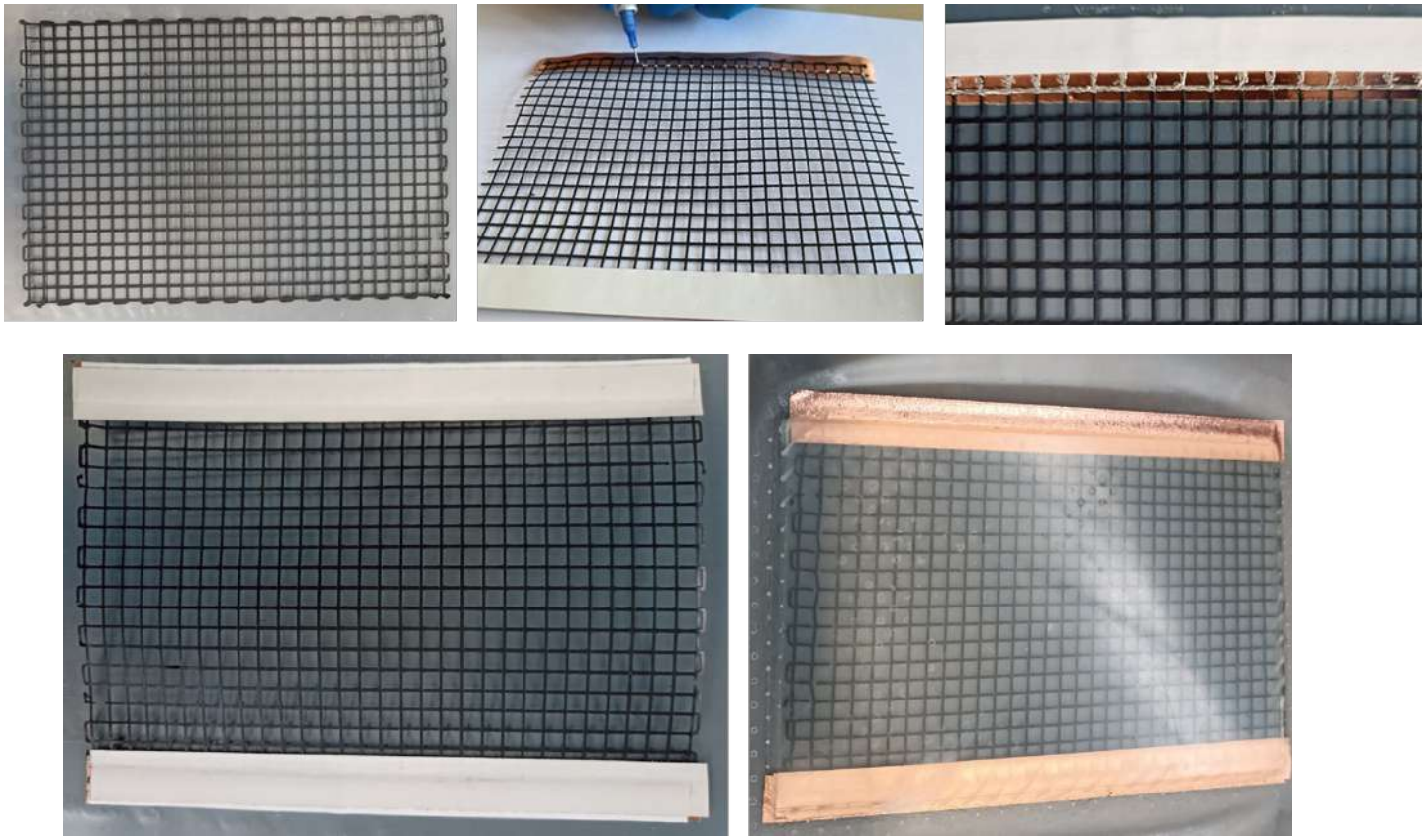

Figure 53 CNT-based grid – connection preparation and GRFP element with embedded heater

TASK 7 – DEMONSTRATOR (LEADER: DRESDEN)

The demonstrators were manufactured in the laboratory using glass fibres and epoxy-based prepreg technology, taking into account the desired component geometries and the requirements of the testing facilities. Their geometry was based on standardized NACA0012 airfoil profiles with a thickness of 30 mm and a length of 300 mm. The profile width was increased from 80 mm to 160 mm in order to enlarge the testing area.
Based on previous work done in the project, resistive heaters made from thermoplastic fibres doped with CNTs (TPF) were selected as the most effective system for demonstrating the de-icing technology. Figures 7.1a–c show the NACA0012 profiles with integrated fibrous thermoplastic heating wires, visible as black lines along the leading edge (Fig. 7.1a–c) and along both the profile contour and the leading edge (Fig. 7.1b). The exposed cables outside the airfoils serve as connection points between the embedded heaters and the power supply equipment. The heaters embedded in the leading edge were designed to prevent ice accumulation, while the

heaters positioned further aft provide protection against the refreezing of meltwater before it can be removed from the airfoil structure.

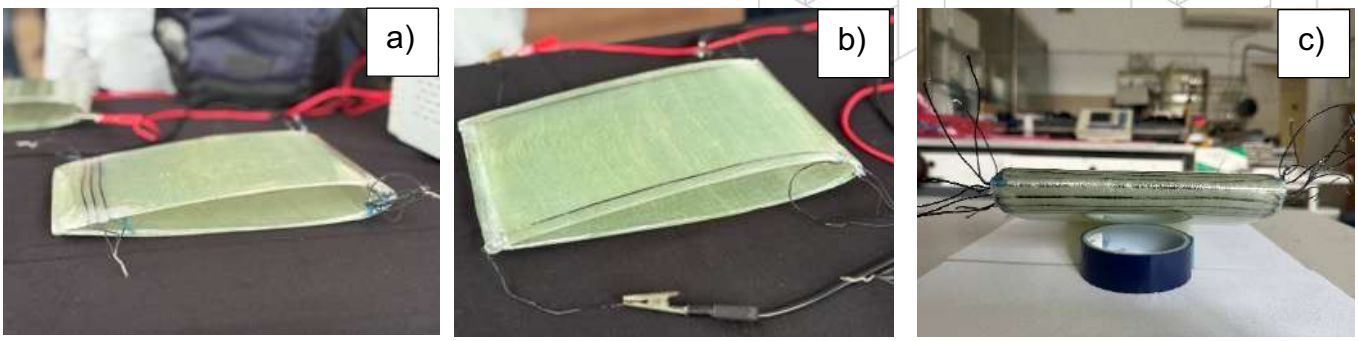

Figure 54: GFRP NACA0012 profiles demonstrators with embedded thermoplastic wires doped with CNTs as heaters: a) heaters on the leading edge and in the run back ice zone; b) heaters on the leading edge and along the edge; c) leading edge with embedded heaters view.

Next, the testing setup was configured, and the power supply parameters were adjusted to ensure efficient operation of the heaters embedded within the profiles. Figure 7.2 presents the preliminary testing arrangement as well as the first infrared (IR) camera images, which illustrate the initial distribution of heat during the early phase of the tests. The colour variations captured by the IR camera indicate differences in temperature: warmer regions shift from purple to white, while unheated areas remain blue.

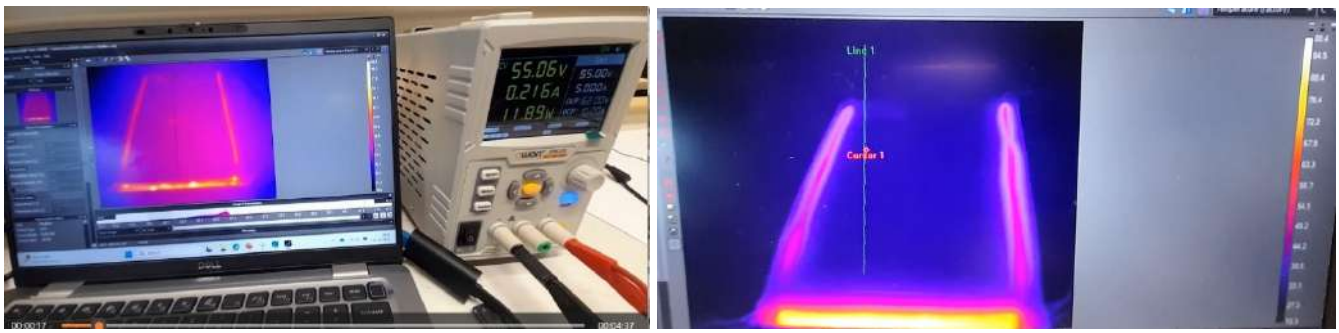

Figure 55: Set of parameters for testing of heating efficiency of GFRP' NACA0012 profiles demonstrators

Figures 7.3a–c present the results of the heating system performance during the testing procedure. A significant increase in temperature is clearly visible in the regions containing the embedded fibrous heaters. Importantly, the heat distribution along the heaters is homogeneous, with no evidence of heating discontinuities or surface areas on the NACA profile that fail to reach elevated temperatures.

Following activation of the power supply, temperature measurements showed a rise in surface temperature to approximately 90–100 °C (Fig. 7.3a, b), with a maximum of around 110 °C observed in Fig. 7.3c. These results demonstrate the high efficiency of the heating system designed and fabricated by TPF and WUT, providing substantial surface temperature increases while requiring relatively low power input as an essential feature for de-icing support systems commonly used in aviation and renewable energy applications.

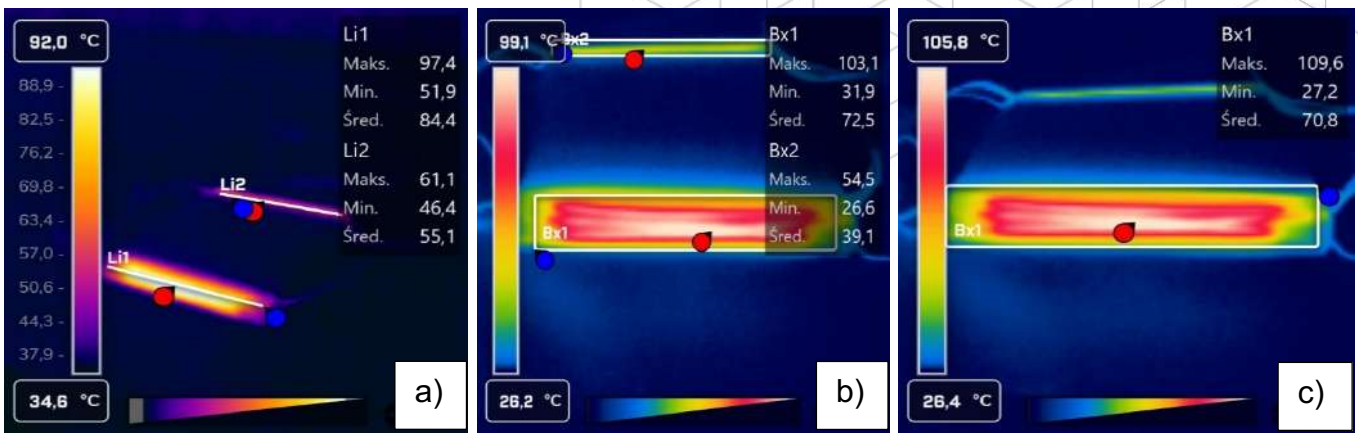

Figure 55: GFRP NACA0012 profiles demonstrators with indicated temperature propagation using IR camera

After the positive results obtained for the airfoils under static, room-temperature testing conditions, the project team shifted its focus to evaluating the efficiency and behaviour of the airfoils under dynamic conditions in the icing wind tunnel facility operated by the TPF partner. The laboratory's open-loop icing wind tunnel allows for various component tests within a chamber measuring 200 × 200 × 600 mm (W × H × L), under conditions closely resembling real-world icing environments. In addition, the facility enables precise control and adjustment of key testing parameters, including air flow speed of up to 60 m/s, chamber temperature ranging from 0 °C to –25 °C, liquid water content (LWC), and median volume diameter (MVD) of the droplets.

Figure 56: Icing wind tunnel set up and tests parameters of power supply

Table 7.1 presents testing parameters of the airfoils during wind tunnel testing campaign in order to verify high efficiency of heaters to melting ice in dynamic conditions.

Table 7.1. Testing conditions of icing wind tunnel and power supply

Device	Wind speed [m/s]	Chamber temperature [°C]	LWC [g/m3]
Icing wind tunnel	20	-5 C	0.2
Device	**Voltage [V]**	**Current [A]**	**Power [W]**
Power supply	60	0,636	38

Figure 7.5 presents installed in the tunnel's testing chamber NACA0012 profile with embedded thermoplastic heaters ready for efficiency investigations, Fig. 7.5a presents view from eagle eye on the edge, while Fig. 7.5b shows bottom side of the profile.

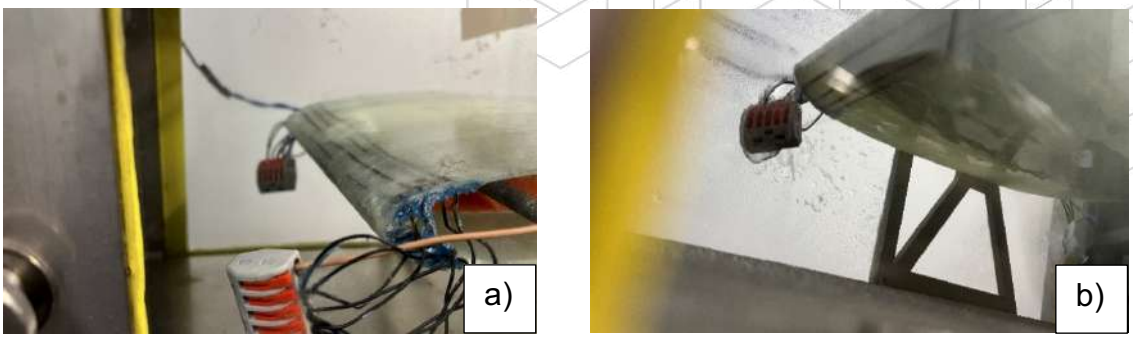

Figure 57: Icing wind tunnel testing campaign with visible heated leading edge during test, a) eagle eye view of the leading edge; b) bottom view of NACA profile.

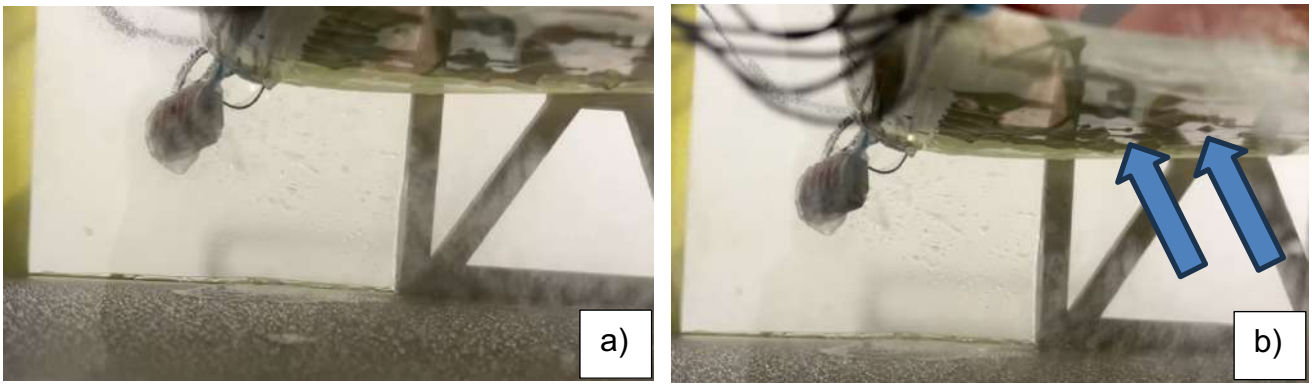

Figure 58: Icing wind tunnel testing campaign with visible heated leading edge during test.

Figure 7.6 shows the testing area from the underside of the NACA profile. In Fig. 7.6a, ice accumulation is visible both on the leading edge and in the region behind it prior to heater activation. In Fig. 7.6b, the situation after activating the heaters during the icing wind tunnel tests is shown. Once the system was activated under the dynamic conditions summarized in Table 7.1, ice melting was observed, evidenced by the presence of water droplets that were not visible before heater activation. These droplets, originating from the melted ice, are indicated with blue arrows in Fig. 7.6b. The presence of meltwater droplets clearly demonstrates that, even under dynamic conditions involving airflow and reduced temperatures, the system was capable of raising the surface temperature above 0 °C, enabling ice melting. This confirms the high efficiency of the active system designed and fabricated by TPF and WUT.

4. SUMMARY AND CONCLUSIONS

- Thermoplastic fibres doped with carbon nanotubes (CNTs) were designed, developed, and successfully integrated as resistive heaters capable of generating high surface temperatures within composite NACA0012 profile demonstrators. These fibres exhibited satisfying properties, enabling efficient heat generation while maintaining compatibility with the composite manufacturing process. Static laboratory tests confirmed that the heating system was able to raise the surface temperature of the demonstrators to approximately 110 °C, demonstrating strong heating performance with relatively low power consumption.
- During dynamic tests conducted in the icing wind tunnel, the system continued to perform effectively under significantly more demanding environmental conditions. Despite the presence of high air flow velocities, low ambient temperatures, and continuous water droplet impingement, the embedded heaters were capable of raising the surface temperature above 0 °C, enabling ice melting and preventing further ice accumulation. This behavior is essential for de-icing and anti-icing applications, where rapid and reliable thermal response is required to ensure operational safety.
- The combined results of the material development, prototype fabrication, and multi-stage testing clearly demonstrated the feasibility of using CNT-doped thermoplastic fibres as an active heating system for composite structures. The success of the demonstrators provides robust proof of concept, showing that such fibre based heating elements can be effectively integrated into composite components and used as a reliable de-icing solution in sectors such as aviation, wind energy, and other industries where icing remains a critical operational challenge.
- Also, several results were obtained with respect to application of PZT sensors to composite structures monitoring and smart composite structures development were obtained. In particular non-linear effects of guided waves interaction with damage of the structure were examined, both experimentally as well as numerically. In accordance with Capability 2 of the COMP-ECO project, the performance of different techniques of PZT sensors integration with the host structure was examined:
- surface attachment of PZT sensors;
- embedding of PZT sensors in additional technological layer of composite structure which is processed and cured in the same manufacturing process as the structure itself;
- embedding of PZT sensors into internal composite structure.